Critical controls on the formation of contact-style PGE-Ni-Cu mineralization: Evidence from the Paleoproterozoic Monchegorsk Complex, Kola Region, Russia

Bartosz T. Karykowski[*1], Wolfgang D. Maier[1], Nikolay Y. Groshev[2], Sarah-Jane Barnes[3], Pavel V. Pripachkin[2], Iain McDonald[1], Dany Savard[3]*

[1]School of Earth and Ocean Sciences, Cardiff University, Main Building, Park Place, Cardiff CF10 3AT, UK.

[2] Geological Institute of the Kola Science Center of the Russian Academy of Sciences (GI KSC RAS), Fersman Street 14, Apatity, Murmansk Region, Russia 184209

[3]Sciences de la Terre, Université du Québec à Chicoutimi, Chicoutimi, Canada G7H 2B1

*(*corresponding author: E-Mail: bkarykowski@yahoo.com)*

Keywords:

Monchegorsk Complex, layered intrusions, contact-style, sulfide mineralization, PGE-Ni-Cu

Abstract

The Paleoproterozoic Monchegorsk Complex, located in the Russian part of the Fennoscandian Shield, constitutes one of the largest mafic-ultramafic layered intrusions in Europe. The complex hosts extensive contact-style PGE-Ni-Cu sulfide mineralization along its margin, irrespective of the host lithology, which ranges from peridotite to pyroxenite and gabbronorite. The mineralized intervals reach up to 3 ppm Pt + Pd and attain a thickness of up to 50 m in the central portions of the intrusion, thinning towards the periphery.

Our study shows that the key process controlling the size and grade of a contact-style deposit in the Monchegorsk Complex, was the efficiency of sulfide collection in distinct zones of the intrusion. Strongly mineralized basal contacts are always associated with intense brecciation and the presence of large amounts of felsic pegmatite, suggesting a multi-stage emplacement of the mafic-ultramafic succession. Thermal modeling demonstrates that multiple episodes of magma influx are required to allow for significant partial melting of the basement. Moreover, the interaction between magma and basement led to the local addition of water and potentially carbon dioxide to the magma, resulting in partial melting of cumulus phases and a reduction in viscosity of the interstitial melt. This increased the porosity of the mush in the vicinity of the lower intrusion contact, which promoted preferential sulfide liquid accumulation at the base, while the local decrease in magma viscosity facilitated gravitational settling of sulfide droplets. These factors led to an efficient collection of sulfide liquid, especially in the center of the complex, where permeability was maintained the longest due to slower cooling relative to more peripheral parts.

Introduction

Layered intrusions around the world are a major target for metal exploration, as they host the bulk of global platinum-group element (PGE), Cr and V resources. Almost all economic PGE deposits are hosted in laterally extensive, but narrow reefs in the central portions of intrusions, such as in the Bushveld Complex (South Africa), the Great Dyke (Zimbabwe) and the Stillwater Complex (USA). The only known economic non-reef-hosted PGE deposits are the Platreef in the Bushveld Complex and the Roby Zone of the Lac des Iles Complex (Canada). As opposed to reef-style mineralization, the Platreef comprises a relatively thick succession of a variety of mineralized mafic-ultramafic rock types along the basal contact of the complex, which is why this deposit type is termed "contact-style" (e.g., Zientek, 2012). In fact, most large layered intrusions globally host contact-style mineralization of variable thickness and metal concentration, notably the Portimo Complex (Finland), the East Bull Lake Complex (Canada) and the Fedorova-Pana intrusion (Russia), but none of them are exploitable under current market conditions (Iljina, 1994; Peck et al., 2001; Schissel et al., 2002).

Genetic aspects of contact-style mineralization, especially concerning the Platreef, are still under debate. In particular the timing of sulfide saturation relative to the final emplacement has been intensively discussed: some authors argued that the mineralization formed in response to *in situ* contamination by country rocks in spatial proximity to the final emplacement (e.g., Buchanan et al., 1981; Gain and Mostert, 1982), whereas more recent studies suggested that the *in situ* contamination did not play a critical role in triggering sulfide saturation, as several lines of evidence indicate that the magma was sulfide-saturated before final emplacement (Holwell et al., 2014;

Kinnaird et al., 2005; Lee, 1996; Maier et al., 2008; Manyeruke et al., 2005; McDonald and Holwell, 2011; Peck et al., 2001).

Critical factors controlling the size and distribution of these deposits in relation to the unmineralized igneous succession are not fully understood either. Notably, the stratigraphically lowermost portions of a layered complex, mostly represented by a thick peridotitic cumulate, commonly lack contact-style mineralization at the base – only higher up in the sequence do these deposits occur, e.g., Konttijärvi/Ahmavaara, Platreef.

This characteristic also applies to one of Europe's largest layered intrusions, namely the Monchegorsk Complex. It is located approx. 120 km south of Murmansk on the Kola Peninsula of Russia and hosts extensive contact-style PGE-Ni-Cu mineralization. The complex belongs to a group of Paleoproterozoic layered intrusions, occurring across the Fennoscandian Shield, which also includes the Portimo Complex in Finland. Recent exploration in the area, targeting the mineralized contact between the intrusion and the floor rocks, yielded intersections of up to 10.9 ppm Pt + Pd over 5.9 m (Eurasia Mining plc, 2010), for a total of 27.8 Mt of category C1 + C2 mineral reserves at 0.6 ppm Pt and 1.1 ppm Pd, respectively (Eurasia Mining plc, 2017).

In this study, we provide a new perspective on the formation of contact-style PGE mineralization based on a thorough analysis of a range of mineralized basal contacts at different stratigraphic levels of the complex. The detailed compositional and lithological characterization of the mineralization, using mineral chemistry as well as lithophile and chalcophile element geochemistry in conjunction with thermal modeling, allows us to improve the understanding of ore-forming processes associated with the formation of mineralized basal intrusion contacts. Furthermore, these results have important implications for exploration targeting contact-style sulfide mineralization.

Geological Setting

One of the most important periods of global mafic-ultramafic magmatism in Earth's history is the Paleoproterozoic (e.g., Maier and Groves, 2011). Expressions of the magmatic activity are recorded in a number of voluminous layered intrusions, dyke swarms and volcanic suites across the Canadian and the Fennoscandian Shield in northern Europe (Vogel et al., 1998). On the basis of coeval magmatism, Bleeker and Ernst (2006) suggested that the Fennoscandian Shield was situated along the southern margin of the Superior Craton at the end of the Archean. The tectonic setting as well as the mantle source of magmatism remain under debate, but most researchers prefer a rift-related mantle plume melting model followed by large-scale contamination with older felsic crustal rocks to explain the trace element and isotopic signature of the igneous rocks (Amelin et al., 1995; Barnes et al., 2001; Ciborowski et al., 2015; Hanski et al., 2001b; Puchtel et al., 1997; Yang et al., 2016).

Several studies have demonstrated considerable petrological and stratigraphic similarities between the layered intrusions on both shields (Iljina and Lee, 2005; James et al., 2002; Schissel et al., 2002). The Fennoscandian layered intrusions, however, seem to be more significant with respect to PGE, Ni, Cu, Cr and V mineralization. Several well-known PGE and Cr occurrences as well as sub-economic to economic deposits are associated with the Finnish intrusions, whereas base and precious metal mineralization in the Russian part of the Fennoscandian Shield are less prominent, despite a long history of mining and exploration going back to the 1930s. These intrusions host a spectacular range of mineralization styles, ranging from stratiform chromitites and basal contact-style PGE-Ni-Cu mineralization to different types of PGE reefs in the lower and upper portions of the intrusion (e.g., Alapieti et al., 1990;

Chashchin et al., 1999; Huhtelin, 2015; Iljina et al., 1992; Kozlov, 1973; Mutanen, 1997; Schissel et al., 2002; Sharkov and Chistyakov, 2012).

One of the most remarkable Fennoscandian intrusions in terms of mineralization is the 2.5 Ga Monchegorsk Complex as it hosts virtually all deposit types associated with layered intrusions in a single complex. These include dunite-hosted massive chromitite, internal PGE reefs associated with interlayered dunite and pyroxenite as well as evolved leucogabbronorite, PGE-Ni-Cu mineralization at the basal intrusion contact and massive Ni-Cu sulfide mineralization in steeply dipping veins and pods (e.g., Karykowski et al., 2016).

Geology of the Fennoscandian Shield

The Fennoscandian Shield of northern Europe consists of three distinct tectonic units: (1) the Kola Domain, (2) the Karelian Domain and (3) the Belomorian Mobile Belt (Fig. 1). The main episode of continental growth of the Kola Domain occurred in response to terrane accretion from 2.9 to 2.7 Ga (Hölttä et al., 2008). High-pressure granulites from the Belomorian Mobile Belt suggest that the Kola Domain collided with the Karelian Domain at 2.72 Ga, thus producing the Fennoscandian Shield. It records two distinct periods of mantle plume activity associated with intraplate rifting towards the end of the Archean. The first magmatic event occurred only on the Kola Domain, producing the 2.5 Ga layered intrusions Mt. General'skaya, Monchepluton, Main Ridge and Fedorova-Pana (Amelin et al., 1995; Balashov et al., 1993; Bayanova et al., 2010; Groshev et al., 2009; Serov et al., 2007). The second magmatic event affected the entire shield at 2.44 Ga, forming numerous layered intrusions, such as the Kemi, Penikat, Portimo, Koillismaa, Näränkävaara, Koitelainen and Akanvaara intrusions in Finland, the Pyrshin, Imandra Lopolith, Kandalaksha, Kolvitsa, Olanga and Burakovsky in Russia and the Kukkola-Tornio intrusion bordering Sweden and Fin-

land (Alapieti et al., 1990; Amelin et al., 1995). According to Bleeker and Ernst (2006), these two episodes can be correlated with the 2.5 Ga Mistassini and the 2.48 – 2.45 Ga Matachewan events in Canada, respectively.

Geology of the Monchegorsk Complex

The Paleoproterozoic Monchegorsk Complex is located in the Kola Domain of the Fennoscandian Shield (Fig. 1). It was emplaced into Archean high-grade metamorphic basement of the Kola Group, comprising metapelites, quartzites, banded iron formation and minor dioritic gneisses (Rundqvist and Mitrofanov, 1993). The complex is overlain by volcanic and sedimentary rocks of the Strel'na Group, which represent the lowermost unit of the Imandra-Varzuga Greenstone Belt (Melezhik and Sturt, 1994; Vrevskii et al., 2010; Zagorodny et al., 1982). The Monchegorsk Complex comprises two spatially separate intrusions, covering an area of ~ 550 km^2: the predominantly ultramafic Monchepluton (~ 65 km^2) and the mafic Main Ridge (~ 485 km^2), which are separated by the Monchetundra Fault trending northwest (Fig. 2 inset).

The Monchepluton is crescent-shaped and consists of six distinct mountains arranged in two branches. The north-northeast-trending branch, reaching approximately 7 km across, is ultramafic in composition and referred to as "NKT Massif", comprising Mts. Nittis, Kumuzhya and Travyanaya (Fig. 2). The west-trending branch is mafic-ultramafic in composition and slightly longer with 9 km, consisting of Mts. Sopcha, Nyud and Poaz. The intersection of the two branches is occupied by a dunitic body, hosting several massive chromitite layers known as the "Dunite Block", which is considered to belong to the Monchepluton (Smolkin et al., 2004). The total thickness of the Monchepluton is more than 2,700 m, but a continuous stratigraphic profile across the intrusion is difficult to obtain due to tectonic fragmentation of the complex.

A composite profile across the Monchepluton can be subdivided into five major zones: (1) the Peridotite Zone at the base of the complex, reaching ca. 500 m in thickness including the Dunite Block; (2) the Interlayered Peridotite-Pyroxenite Zone, reaching ca. 300 m in thickness; (3) the Pyroxenite Zone with a thickness of more than 750 m; (4) the Noritic Zone in the upper portion of the intrusion with a thickness of at least 450 m and (5) the Gabbroic Zone with a thickness of more than 700 m (the uppermost portion of the intrusion has been eroded), comprising the Vuruchuaivench intrusion, which has been shown to represent the continuation of the underlying Noritic Zone (Rundkvist et al., 2014; Sharkov and Chistyakov, 2012) (Fig. 3).

Lithostratigraphy and nature of mineralization

The stratigraphy of the NKT Massif and Nyud is rather simple lithologically, but highly complex in terms of texture (Fig. 4, 5). Detailed logs of drill cores, intersecting the basal intrusion contact at Nittis and Nyud, are shown in Figure A1.

The Nittis intrusion, as intersected by drill holes MT79 and MT94, comprises a more than 300-m-thick succession of strongly layered orthopyroxenite. The lowermost 7 m of the intrusion constitute a diffuse contact zone characterized by a change in texture from strongly layered to distinctly ophitic orthopyroxenite (Figs. 4 A, A1). Additionally, several lenses, schlieren and patches of felsic pegmatite interlayered with different metasedimentary rocks occur in the lower part of the contact zone (Fig. 4 A, B). Hence, a distinct boundary between the ultramafic intrusion and the Archean basement cannot be defined. The contact zone is further associated with dolerite dykes and veins cross-cutting the complex unit. The bulk of the sulfide mineralization is hosted by the layered orthopyroxenite, covering some 30 m at the base of the intrusion. Moreover, several thin sulfide-rich veinlets occur above the basal mineralized zone (Fig. 4 C, D). In addition to the basal sulfide mineralization, steeply dipping

massive sulfide veins, ranging from 5 cm to 3 m in thickness, occur mainly in the central parts of the intrusions, which were not intersected by drill holes MT79 and MT94 (Figs. 4 E, 5). They may reach a vertical thickness of more than 150 m and can be traced for up to 1.5 km, before they pinch out (Kozlov, 1973).

Stratigraphically deeper portions of Nittis were sampled close to the contact between the Pyroxenite Zone and the underlying Interlayered Pyroxenite-Peridotite Zone (Fig. 5 A-B). A continuous sample set across the latter was collected at Mt. Kumuzhya and comprises olivine-rich lithologies, ranging from harzburgite to orthopyroxenite. Samples from the Peridotite Zone, located at the base of the NKT Massif, were recovered from an abandoned sulfide mine dump at Mt. Travyanaya, exploiting the contact zone between the intrusion and the floor rocks, which is represented by mineralized gabbronorite from the intrusion margin as well as different peridotitic rock types, mainly comprising harzburgite. Additional samples from the Peridotite Zone were collected from an abandoned chromite mine in the Dunite Block. The minimum cumulative thickness of the NKT Massif at the current erosional level is > 1,100 m.

On the basis of historic drilling, Kozlov (1973) reported that the basal mineralized zone generally follows the lower intrusion contact marked by gabbronorite, extending across the entire NKT Massif and Mt. Sopcha (Fig. 5 A-B). Its thickness increases from the peripheral parts of the intrusion towards the center, reaching up to 50 m, with average sulfide contents of 3 to 5 vol % (Dedeev et al., 2002). The mineralized gabbronorite described by Kozlov (1973) is absent in the studied section at Nittis. However, the mineralized gabbronorite from the basal contact of the Travyanaya intrusion may be a representative analogue in terms of texture and composition. Drill holes MT79 and MT94, used for this study, intersected the western part

of the Nittis intrusion, thus representing a more peripheral segment of the mineralized interval (Fig 2).

Moreover, a basal mineralized contact zone has been intersected by drill hole 1815 collared in the peripheral part of the Nyud intrusion (Fig. 5 E-F). The mineralized horizon at Nyud comprises an approximately 20-m-thick unit of sulfide-bearing melanorite, overlying interlayered tonalite with abundant felsic pegmatite veins and schlieren similar to Nittis (Fig. A1). The mineralized melanorite gives way to barren melanorite up-section without a significant change in texture. The visible sulfide abundance is very similar to that at Nittis with approximately 3 vol %. The sulfides mostly occur as relatively small interstitial patches, reaching about 10 mm in diameter, together with minor sulfide-rich veinlets, in particular close to the intrusion contact.

Samples and analytical methods

Weathered portions of outcrop samples were removed prior to crushing, splitting and milling in an agate planetary mill at Cardiff University. After heating each sample for two hours at 900 °C, the Loss on Ignition (LOI) was determined gravimetrically. Fusion digestion with subsequent inductively coupled plasma optical emission spectrometry (ICP-OES) and inductively coupled plasma mass spectrometry (ICP-MS) was used to determine major and trace elements following methods and instrumentation described by McDonald and Viljoen (2006). The platinum-group element (PGE) concentrations were determined at LabMaTer, Université du Québec at Chicoutimi (UQAC), using ICP-MS after nickel-sulfur fire assay, following the analytical protocol outlined by Savard et al. (2010). Analytical precision and accuracy are given in Table 1. Sulfur was analyzed by high-temperature combustion combined

with infrared (IR) spectrometry and sulfur titration, using a Horiba 220V S-C analyzer at LabMaTer, following the methodology outlined by Bédard et al. (2008).

Mineral compositions of olivine, pyroxene and plagioclase were determined, using a Zeiss Sigma HD Analytical Field Emission Gun SEM equipped with two Oxford Instruments 150 mm^2 EDS detectors at Cardiff University. Analyses were carried out using an accelerating voltage of 20 kV, 2.5 nA beam current and a spot size of 2 – 4 μm. The counting time was 30 s for each spot. Natural minerals and synthetic metals from Astimex Ltd. were used for calibration. Olivine, diopside and plagioclase from the same supplier were measured during the analytical runs to monitor instrumental drift.

Results

Petrography

The sample set from the Dunite Block, the NKT Massif and the Nyud intrusion comprises 45 samples, representing lherzolite, harzburgite, olivine-websterite, (olivine-)orthopyroxenite, melanorite, mineralized gabbronorite, felsic pegmatite and basement lithologies.

The lherzolite is a coarse-grained mesocumulate with 60 to 65 vol % olivine, 25 to 30 vol % orthopyroxene and 10 to 15 vol % poikilitic clinopyroxene. In addition to approximately 1 vol % chromite, the rock also contains minor interstitial plagioclase, whereas sulfides are completely absent. The only occurrence of this rock type is in the Dunite Block, representing the lowermost portion of the Peridotite Zone (Fig. 3).

The harzburgite is a fine- to medium-grained mesocumulate with 50 to 85 vol % olivine, 10 to 45 vol % orthopyroxene and minor clinopyroxene as well as plagioclase. The rock type is only present in the Interlayered Pyroxenite-Peridotite Zone at

Kumuzhya and in the Peridotite Zone exposed at Travyanaya (Fig. 5 A-B). Harzburgite from the latter hosts disseminated interstitial sulfide mineralization and thin sulfide veinlets cross-cutting the rock (Fig. 6 A). The total amount of sulfide reaches about 2 vol %.

The olivine-websterite is a medium- to coarse-grained orthocumulate with approximately 65 vol % orthopyroxene, 15 vol % olivine, 7 vol % clinopyroxene and 8 vol % plagioclase. It only occurs in the lowermost portion of the NKT Massif exposed at Travyanaya. The analyzed sample is also characterized by abundant disseminated interstitial sulfide blebs, which reach up to 5 mm across and account for ~ 5 vol %.

The layered orthopyroxenite is an adcumulate with 70 to 90 vol % orthopyroxene and is only present at Nittis and Kumuzhya. Orthopyroxene occurs as highly elongated crystals of up to 10 mm with an aspect ratio of up to 9:1 (Fig. A2). Additionally, much smaller equant cumulus orthopyroxene is present in between the elongated ones, reaching 1 mm in diameter (Fig. 7 A). Anhedral plagioclase accounts for < 10 vol % and occurs interstitial to the orthopyroxene. Clinopyroxene reaches up to 5 vol % and mostly forms small blebs within or along the margins of orthopyroxene. Moreover, large poikilitic grains interstitial to orthopyroxene are present. Olivine occurs only in a few samples, especially in those from Kumuzhya and the lower portions of the Nittis intrusion, where it accounts for up to 30 vol %. It is mostly subhedral, reaching up to 1 mm across. Most of the samples contain minor amounts of subhedral chromite. Sulfides generally occur in relatively large interstitial patches of up to 10 mm, comprising pyrrhotite, pentlandite and chalcopyrite with minor pyrite (Fig. 6 B).

The ophitic orthopyroxenite is mineralogically similar to the layered orthopyroxenite described above. Its texture, however, is distinctly ophitic, defined by

randomly oriented lath-shaped orthopyroxene crystals with interstitial plagioclase. This rock type is commonly brecciated and intruded by mineralized layered orthopyroxenite, but it is not mineralized itself and only present in the basal contact zone of the Nittis intrusion.

The melanorite occurs exclusively at Nyud and shares many similarities with the layered orthopyroxenite from Nittis; however, the former is characterized by a higher modal abundance of mostly poikilitic plagioclase, ranging from 10 to 25 vol % (Fig. 7 B). Additionally, the mineral lamination is not as strongly developed as in the orthopyroxenite due to lower aspect ratios of the orthopyroxene crystals. Clinopyroxene is generally present as patchy oikocrysts, accounting for less than 5 vol %. Olivine is absent, whereas chromite occurs only as an accessory phase.

The mineralized gabbronorite is a medium-grained rock type with a distinctly ophitic texture defined by up to 4-mm-long plagioclase laths, accounting for ~ 55 vol %, whereas poikilitic clino- and orthopyroxene comprise ~ 30 and 12 vol %, respectively. Interstitial sulfide is spatially associated with pyroxene and reaches up to 2 vol % (Fig. 6 C).

The felsic pegmatite is always associated with the contact between the mafic-ultramafic rocks and the basement. It is a highly variable rock type in terms of grain size as it ranges from very coarse- to fine-grained over short distances (Fig. 7 C). It generally consists of anhedral quartz and feldspar with minor amounts of mica. Locally, these minerals may form symplectites.

The country rock at the base of the NKT Massif is a relatively variable metasediment, consisting of different proportions of mica, chlorite, staurolite, quartz and feldspar, which form a strongly banded mica schist (Fig. 7 D). Fragments of this rock type frequently occur within orthopyroxenite close to the basal contact of the Nittis

intrusion. In addition, these metasediments may contain up to 7 vol % sulfide over an interval of 2 m close to the intrusion contact, primarily comprising pyrrhotite with minor chalcopyrite and pentlandite. The same sulfide assemblage also occurs in gray tonalite, where it is in direct contact with the Nyud intrusion.

Mineral chemistry

The mineral chemistry of rock-forming minerals was determined in a set of 34 samples from the Dunite Block, the NKT Massif and the Nyud intrusion. The full dataset of mineral compositions is available in Table A1. As a result of the ubiquitous presence of cumulus orthopyroxene, the most suitable proxy for tracing the degree of fractionation is the Mg# of orthopyroxene (100 x molar Mg/(Mg+Fe)). A corresponding stratigraphic profile across the Monchepluton is shown in Figure 3. The Mg# of orthopyroxene covers a relatively small range at Nittis, varying from 84 in orthopyroxenite to 89 in the most primitive olivine-orthopyroxenite (sample 15NMAS-1) with Cr concentrations from 4,000 to 4,800 ppm (Fig. 8). The Kumuzhya intrusion features slightly more magnesian orthopyroxene with Mg# ranging from 88 to 89 and up to 4,600 ppm Cr. The most primitive orthopyroxene compositions were measured in a harzburgite from Travyanaya, reaching Mg# = 91 with up to 5,000 ppm Cr. The Nyud intrusion is generally characterized by lower Mg# with an average of 83 and 3,400 to 3,900 ppm Cr. The Mg# of clinopyroxene from the NKT Massif varies from 84 to 91, whereas clinopyroxene from the Nyud intrusion has an Mg# of 85. Olivine from the NKT Massif covers a range in forsterite contents from Fo_{82} to Fo_{87}. Only chromite-rich dunite and lherzolite from the Dunite Block have even more magnesian olivine with Fo_{92} and Fo_{89}, respectively. The stratigraphic variation in mineral chemistry across the Nittis intrusion shows a distinct approximately

200-m-thick basal compositional reversal in orthopyroxene composition (Fig. 11), which is also evident in clinopyroxene and olivine compositions (not shown).

Lithophile element geochemistry

A total of 57 samples, covering the Dunite Block, the NKT Massif and Nyud, were analyzed for lithophile elements. The full dataset of whole rock geochemical analyses can be found in Table A2.

The major element composition of the analyzed samples is primarily controlled by variations in the modal proportion of rock-forming minerals. Peridotites from Kumuzhya, Travyanaya and the Dunite Block are mainly characterized by high modal proportions of olivine with varying amounts of ortho- and clinopyroxene, as reflected in the high MgO concentrations of more than 40 wt % (Fig. 9 A, B). Notably, the peridotites show a bimodal distribution in terms of Cr concentrations, reflecting distinct differences in chromite abundance (Fig. 9 C). Kumuzhya orthopyroxenites generally feature higher modal proportions of orthopyroxene relative to olivine, resulting in slightly lower MgO concentrations, ranging from 33 to 38 wt %. Nittis orthopyroxenites have distinctly lower MgO contents of 17 to 28 wt %, as they are mainly composed of orthopyroxene with varying proportions of plagioclase, whereas clinopyroxene and olivine are minor components. The analyzed melanorites from Nyud have 16 to 25 wt % MgO due to slightly higher modal proportions of plagioclase compared to Nittis orthopyroxenites. Chromium concentrations are also slightly lower at Nyud. The mineralized gabbronorite from Travyanaya has the lowest MgO and Cr concentrations with 8 wt % and < 300 ppm, respectively. Notably, the analyzed samples from Nittis and Nyud show considerable overlap with mafic-ultramafic rocks from the Fedorova-Pana intrusion (Schissel et al., 2002); however, the latter have consistently higher CaO concentration due to slightly higher modal abundances

of clinopyroxene (Fig. 9 A, B). Lithologies similar to those from Travyanaya or the Dunite Block with > 34 wt % MgO seem to be absent in the Fedorova-Pana intrusion. A broadly positive correlation between whole rock Mg# and Cr/V ratios is evident among the analyzed chromite-poor lithologies, allowing for a comparison of the different intrusions with respect to the degree of fractionation (Fig, 9 D).

In terms of primitive mantle-normalized incompatible trace element patterns, most mafic-ultramafic samples have fractionated patterns with strongly negative Nb-Ta and minor Ti anomalies (Fig. 10 A - E). Moreover, many of them feature minor positive Zr-Hf and variable P anomalies. Only samples from the lowermost part of Nittis and a distinctly ophitic orthopyroxenite, associated with the mineralized zone, are characterized by relatively unfractionated incompatible trace elements with strongly positive Zr-Hf anomalies, whereas the Nb-Ta anomaly in these rocks is rather subtle to absent (Fig. 10 B). These compositions are remarkably similar to rocks from the Sompujärvi (SJ) Reef in the Penikat intrusion (Maier et al., in review). The melanorites from Nyud, however, show a strong overlap with orthopyroxenites from Nittis and the mineralized gabbronorite from Travyanaya (Fig. 10 C). Olivine-rich lithologies, such as olivine-orthopyroxenite from Kumuzhya and lherzolite from the Dunite Block, have generally lower total incompatible trace element concentrations and are distinct from the Nittis orthopyroxenites as well as Nyud melanorites (Fig. 10 D). In contrast, harzburgite from Kumuzhya and Travyanaya plot between orthopyroxenites from Nittis and lherzolites from the Dunite Block, reflecting slight differences in modal olivine/pyroxene ratios (Fig. 10 E). The mineralized metasediment from Nittis as well as the mineralized tonalite from Nyud both have typical upper crustal incompatible trace element patterns with a strong enrichment in light rare earth elements (REE) relative to heavy REE (Fig. 10 F). Felsic pegmatite from the

intrusion contact shows extremely negative Ti anomalies in comparison to the associated basement lithologies.

Downhole geochemical data along a composite profile across the peripheral portion of the Nittis intrusion show a distinct upward increase in whole rock MgO concentrations and Cr/V ratios, whereas Al_2O_3 contents decrease significantly (Fig. 11). La/Nb ratios mostly range from 2 to 3; however, close to the basal contact, the ratio increases gradually towards the pegmatite. The only exception is an ophitic orthopyroxenite sample with exceptionally high Cr/V and low La/Nb ratios.

Chalcophile elements

Magmatic sulfides are generally assumed to be the primary host for chalcophile metals in layered intrusions. The analyzed sample set from the Dunite Block, the NKT Massif and the Nyud intrusion shows a broadly positive correlation between chalcophile metals and S, confirming sulfide as the main control on chalcophile metal abundances (Fig. 12 A - E). Variations in correlation between Ni and S can be partly attributed to Ni hosted in olivine, whereas elevated Ir concentrations result from high modal abundances of chromite (i.e., Dunite Block). The correlation between Cu, Pt, Pd and S, however, becomes notably poorer in samples with less than 1,000 ppm S, which is also evident in the negative correlation between Cu/S, Pt/S and S in this sample subset (Fig. 12 F, G). A plot of Pd/Pt vs. Pd/Ir shows that both Pd and Pt as well as Pd and Ir are fractionated (Fig. 12 J). Variations in Pd/Ir ratios can be explained by chromite crystallization and monosulfide solid solution (mss) fractionation, whereas changes in Pd/Pt ratios are difficult to account for (Fleet et al., 1993; Puchtel and Humayun, 2001).

Notably, a group of samples plots away from the general trend; they are characterized by anomalously high PPGE (Pd, Pt, Rh) and low IPGE (Ir, Os, Ru), resulting

in elevated PPGE to IPGE ratios (Fig. 12 E, I, K). All of these samples represent sulfide veins of variable thickness cross-cutting the layered succession containing interstitial sulfides.

Drill core profiles, intersecting the mineralized contact of the Nittis and Nyud intrusions, show that significant sulfide accumulation (up to 5 wt % S) is exclusively associated with the basal contact zone of each intrusion (Fig. 13 A, B). These zones are characterized by elevated base metal concentrations, reaching up to 2 wt % Cu and Ni each, and 0.15 wt % Co, whereas precious metal concentrations may be as high as 3.3 ppm Pt + Pd. Moreover, basement lithologies at both intrusions are mineralized in spatial proximity to the mafic-ultramafic rocks. Another remarkable zone of mineralization was intersected some 100 m above the basal contact of Nittis. The mineralization is hosted in several thin sulfidic veinlets, cross-cutting the orthopyroxenitic cumulate over a vertical thickness of about 3 m, and reaches up to 32.8 ppm Pt + Pd (Fig. 4 D). Sulfur concentrations are relatively low across the mineralized interval, which is why the mineralization is difficult to distinguish macroscopically.

All rocks from the NKT Massif and the Nyud intrusion have > 20 ppb Pt + Pd, indicating that they crystallized from a magma, which was saturated in sulfide (Figs. 12 C, D, 13). In addition, Cu/Pd ratios in the mafic-ultramafic rocks are generally below the primitive mantle value, reflecting the presence of cumulus sulfide (Fig. 13). In contrast, samples from the Dunite Block have < 15 ppb Pt + Pd, which is consistent with a crystallization from a sulfide-undersaturated magma (Fig. 12 H).

This is particularly evident in primitive mantle-normalized chalcophile element patterns of the analyzed samples as chromite-poor lherzolite from the Dunite Block has generally low PGE concentrations and almost flat patterns with Pd/Ir ratios below

6, supporting a lack of cumulus sulfide, whereas harzburgite from Travyanaya has higher PGE concentrations and features an enrichment in PPGE relative to IPGE with positive Pd as well as Rh anomalies and a high Pd/Ir ratio of more than 75 (Figs. 12 J, 14 A). Chromite-rich dunite from the Dunite Block exhibits a strong enrichment in IPGE relative to PPGE, which reflects the presence of IPGE-rich cumulus chromite (e.g., Capobianco and Drake, 1990).

All other lithologies from Travyanaya, ranging from websterite to orthopyroxenite and gabbronorite, have remarkably similar patterns with Pd/Ir ratios from 48 to 65 and positive Pd as well as Rh anomalies (Fig. 14 B). Kumuzhya, Nittis and Nyud lithologies also show positive Pd and Rh anomalies and relatively high Pd/Ir ratios of more than 20 (Fig. 14 C, D, E). Only the ophitic orthopyroxenite from Nittis has a different pattern lacking distinct anomalies. It is worth noting that the positive Pd and Rh anomalies are characteristic of many other Fennoscandian intrusions of similar age, such as the Portimo Complex, and also in parts of the Great Dyke of Zimbabwe and the Muskox intrusion in Canada (Barnes and Francis, 1995; Iljina et al., 1992; Maier et al., 2015). The mineralized metasediment from Nittis as well as the mineralized tonalite from Nyud show similar chalcophile element patterns to the mineralized melanorite and orthopyroxenite from the respective intrusions, which suggests a common origin of the sulfide mineralization (Fig. 14 F). Notably, the mineralized tonalite is also distinct in its pattern from the barren one, despite similar lithophile element chemistry.

In contrast to the interstitial PGE-Ni-Cu mineralization, characterized by Pd/Ir ratios, ranging from 20 to 600, and strongly positive Pd as well as Rh anomalies, sulfide veins from Travyanaya and Nittis have completely different patterns with much higher Pd/Ir ratios, starting above 2,500 and reaching up to 18,000 (Fig. 14 G, H).

Additionally, the positive Rh anomalies are not as pronounced and may also be absent in the most fractionated samples. These veins strongly resemble massive sulfide mineralization associated with micronorites from Nyud (Fig. 14 G).

Discussion

Emplacement mode: liquid or crystal-mush?

Many layered intrusions and mafic sills are characterized by a basal compositional reversal, in which whole rock and mineral compositions become progressively more primitive towards the center of the intrusion or sill. A number of studies have shown that these basal reversals provide valuable insight into the processes associated with the emplacement of mafic-ultramafic intrusions (e.g., Alapieti, 1982; Campbell, 1978; Lightfoot et al., 1984; Page, 1979).

Key features of the basal reversal at Nittis are an upward increase in the Mg# of orthopyroxene, whole rock MgO concentrations and Cr/V ratios, which are mirrored by decreasing Al_2O_3 concentrations. Moreover, La/Nb ratios remain relatively consistent across the pyroxenitic part of the profile (Fig. 11).

Several models for the origin of these reversals have been proposed, ranging from the crystallization of compositionally diverse liquids as a result of *in situ* contamination or magma stratification to the crystallization of crystal-liquid mixtures, affected by crystal settling, flow differentiation, convection and variable amounts of trapped liquid (see Latypov, 2003 for a review).

In situ contamination of a crystal-poor parental magma with the immediate host metasediments would have considerably affected the incompatible trace element signature of the magma, especially close to the intrusion contact, where the degree of contamination would have been the highest. The near-constant La/Nb ratios across

most of Nittis, however, argue strongly against *in situ* contamination as the principle mechanism for the development of a basal reversal. Only sample 79-145, which is in direct contact with the host metasediment, has a slightly elevated La/Nb ratio, indicating that the extent of *in situ* contamination is confined to the immediate surroundings. This is further supported by Bekker et al. (2016), who noted a slightly stronger mass-independent fractionation of sulfur isotopes in NKT Massif samples from the intrusion contact relative to those from the intrusion center.

Additionally, the highly elongated crystal shape of orthopyroxene, defining the typical mineral lamination of the Nittis pyroxenites, is unlikely to have formed *in situ* during the crystallization of a liquid (Fig. 7 A). The upward increase in whole rock MgO concentrations together with the antithetical behavior of Al_2O_3 reveal a distinct shift in modal mineralogy with stratigraphic height. As orthopyroxene is the only cumulus phase, the Al_2O_3 concentrations, reflecting the abundance of interstitial plagioclase, can be used as a proxy for the amount of trapped liquid (Fig. 11). The highest Al_2O_3 concentrations and therefore amount of trapped liquid occur at the basal contact of the intrusion and subsequently decrease towards the top of the succession. It is difficult to explain these features with the crystallization of a crystal-poor liquid as this would have produced distinct variations in the grain size of orthopyroxene and plagioclase as a function of cooling rate. Orthopyroxene in the layered orthopyroxenite, however, does not show any systematic changes in grain size from the intrusion contact to the center and plagioclase remains an interstitial phase. Moreover, the ubiquitous presence of sulfide-saturated lithologies and the homogeneous large-scale distribution of cumulus sulfide in peridotites, pyroxenites and norites is also inconsistent with an initially crystal-poor magma chamber as gravity-driven sulfide settling would be expected under these conditions.

The basal reversal can thus be best explained by a decreasing trapped liquid component away from the intrusion contact, whereby original liquidus compositions of orthopyroxene were modified by reaction with trapped liquid (e.g., Barnes, 1986a). This may not only affect major elements, but also trace elements, such as Cr and V. The extent of the modification depends on the amount of trapped liquid as indicated by the negative correlation between the Mg# of orthopyroxene as well as the Cr/V ratios and the whole rock Al_2O_3 concentrations – the higher the amount of trapped liquid, the higher the extent of modification.

Thus, the geochemistry of the basal reversal helps to constrain the emplacement mode of the NKT Massif. Our data are consistent with a model in which the intrusion was emplaced as a crystal mush with relatively high amounts of suspended cumulus orthopyroxene. Close to the intrusion margins, elevated cooling rates hindered effective and thorough gravitational settling of orthopyroxene, resulting in high amounts of trapped liquid. As cooling rates generally decrease away from the intrusion contact, the amount of interstitial liquid trapped in the cumulate was also lower, as reflected in the smaller trapped liquid shift (Fig. 11).

Genetic aspects of contact-style PGE-Ni-Cu mineralization at Monchegorsk

Cross-cutting relationships in drill core together with relative abundance and geochemical data indicate that the earliest pulse of magma, intruding relatively cold basement lithologies underlying the Monchegorsk area, was volumetrically insignificant, yet important for the formation of sulfide mineralization. It is represented by the ophitic orthopyroxenite, which has the most primitive composition of all Nittis lithologies and seems to have crystallized from a sulfide-undersaturated magma with a distinct La/Nb ratio close to that of the primitive mantle (Fig. 11). Even though the first pulse of magma did not contribute any sulfides, it introduced considerable heat

into the basement, resulting in an increased ambient temperature (Fig. 15 A). The second phase of magmatism was much more significant in terms of volume and caused intense brecciation of the ophitic orthopyroxenite. The ubiquitous presence of sulfide-saturated rocks across the NKT Massif and the Nyud intrusion requires an early sulfide saturation event, prior to final emplacement, most likely in a staging magma chamber (Fig. 15 B). After reaching sulfide saturation, the sulfide droplets were enriched in PGE, while interacting with the magma, and eventually settled to the base of the staging chamber together with crystallizing olivine and orthopyroxene. This protocumulate, consisting of cumulus olivine, orthopyroxene, liquid sulfide and residual silicate melt, was episodically remobilized and crudely density-sorted within the crystal mushes as it was transported into higher crustal levels. Upon final emplacement of these large volumes of crystal mush, the preheated basement underwent not only partial melting, as reflected in the frequent occurrence of felsic pegmatite, but also devolatilization, which led to the local addition of water and potentially carbon dioxide to the magma (Fig. 15 C).

The effect of this is twofold: (1) the added volatiles act as fluxes, thus lowering the melting point of the cumulus minerals, which results in local small-scale dissolution of these cumulus phases within the crystal mush, and (2) it reduces the viscosity of the interstitial melt. Although Mg-rich orthopyroxene has a high liquidus temperature, thermodynamic considerations suggest that the melting temperature of cumulus orthopyroxene can be readily suppressed to less than 1,100 °C in the presence of plagioclase and water.

On the one hand, local melting of cumulus phases resulted in an enhanced porosity of the crystal mush in the vicinity of the lower contact, promoting preferential sulfide liquid collection at the base of the intrusion. On the other hand, the local de-

crease in magma viscosity facilitated the gravitational settling of sulfide droplets. Together with the basement preheating and the associated lower cooling rate, these factors led to a relatively efficient accumulation of sulfide, especially in the center of the intrusion, where permeability was maintained the longest due to slower cooling relative to more peripheral parts (Fig. 15 D). In some places, the settling sulfide liquid also percolated into the basement as reflected in the mineralized basement lithologies at Nittis and Nyud (Fig. 14 F). The migration of sulfide liquid has also been observed in many other intrusions, such as the Portimo Complex, where the mineralization extends for several tens of meters into the basement (Iljina et al., 1992). Despite generally low modal sulfide abundances of up to 5 vol % in these basement lithologies, the sulfide liquid may have percolated into the footwall through an interconnected sulfide network, which may develop at even lower sulfide abundances (Godel, 2013).

Constraining the composition of the parental magma is rather difficult as chilled margins have not been observed in the Monchegorsk Complex. The Mg# of the parental magma, however, can be calculated with the Mg-Fe olivine-liquid partition coefficient of 0.30, using the most primitive olivine composition from the NKT Massif (Roeder and Emslie, 1970). Forsterite contents reach up to 87.2 mol % in olivine from the NKT Massif, which corresponds to a parental magma with Mg# = 67.1. This composition is similar to siliceous high-Mg basalts (SHMB) that are considered to represent the parental magma for other Paleoproterozoic intrusions, such as the Portimo Complex (Saini-Eidukat et al., 1997). Moreover, Paleoproterozoic picrites in northern Finland analyzed by Hanski et al. (2001a) have a similar Mg#, averaging at 66.7 (n = 3).

The poor correlation between Cu, Pt, Pd and S in samples with relatively low S concentrations has been observed in many intrusions, similar to samples from this

study with less than 1,000 ppm S (Fig. 12 B, C, D, F, G), which is generally attributed to late magmatic or hydrothermal S loss (e.g., Cawthorn and Meyer, 1993; Maier and Barnes, 1996). In contrast, the positive correlation between Pt and Pd as well as Ir and Pd suggests limited mobility of the PGE as Pd may behave mobile, while Pt and Ir are generally regarded as immobile elements (Fig. 12 H, I).

Therefore, assuming a picritic parental magma containing 498 ppm Ni, 86 ppm Cu, 9.54 ppb Pd and 0.76 ppb Ir (see Barnes and Lightfoot, 2005), the chalcophile element chemistry of the contact-style mineralization can be explained by sulfide segregation at R factors between 1,000 and 10,000 with limited fractional crystallization of the sulfide liquid (Fig. 16). It is worth noting that the mss component is rather underrepresented in the dataset, possibly indicating further mss-rich sulfide mineralization at depth.

Thermal modeling of basement preheating

Distinct geochemical and textural characteristics of the intersected ophitic orthopyroxenite, together with complex cross-cutting relationships at the base of Nittis, indicate that this rock type may represent a volumetrically minor first pulse of magma intruding into the crust. This pulse may have introduced significant heat into the basement, allowing for relatively slow cooling of the second major intrusive event, which led to effective sulfide collection at the base of the complex. This hypothesis can be tested numerically, assuming conductive heat transfer by using the explicit finite difference method. Discretization of Newton's one-dimensional heat diffusion equation yields:

$T_i^{n+1} = T_i^n + \kappa\Delta t\left(\frac{T_{i+1}^n - 2T_i^n + T_{i-1}^n}{(\Delta x)^2}\right)$, where κ is the thermal diffusivity (κ = 2 x 10^{-6} m^2s^{-1}). A detailed derivation of the one-dimensional explicit heat function togeth-

er with the respective boundary conditions for the model can be found in Electronic Appendix 1.

The intention of the model is to evaluate two possibilities:

(1) Intrusion of a 1500-m-thick crystal mush into preheated basement
(2) Intrusion of a 1500-m-thick crystal mush into cold basement

The preheating of the basement was modeled assuming the intrusion of multiple sills with an average thickness of 50 m and a spacing of 250 m from approximately 2 to 4 km depth, as shown in Figure 17 A. The intruding sills were assumed to have a temperature of 1200 °C (e.g., Huppert et al., 1985). The model shows that these thin sills cool relatively quickly, reaching less than 800 °C after 10 years; however, basement temperatures in excess of 700 °C are only attained in close vicinity of the sills (< 5 m). Nevertheless, these sills are capable of raising the average basement temperature from less than 120 °C to more than 350 °C across the intruded basement thickness (Fig. 17 A).

In a second step, it was assumed that the main pulse of magma, which produced the NKT Massif, was emplaced with a temperature of 1200 °C into preheated basement at a depth of 2.5 km, as shown in Figure 17 B. The frequent occurrence of felsic pegmatite close to the intrusion contact strongly suggests partial melting of the immediate basement, but dehydration melting requires temperature in excess of 700 °C (e.g., Singh and Johannes, 1996). The model indicates that this temperature is reached up to 50 m away from the intrusion contact after 100 years and even 120 m away after 1000 years. Therefore, dehydration melting may also affect distal regions of the basement, given that the latter is preheated.

Alternatively, it may be assumed that the main pulse of magma was emplaced into cold basement, while all other variables remained unchanged. In this case, a geothermal gradient of 30 K/km was used for the basement temperature profile. The

thermal modeling in Figure 17 C illustrates that basement temperatures in excess of 700 °C can only be attained directly at the intrusion contact upon emplacement. As a consequence, only insignificant volumes of pegmatite would be produced at the contact, which cannot account for the high abundance of pegmatite observed in drill core. Afterwards, temperatures gradually decrease from 700 °C, indicating much higher cooling rates compared to the emplacement into a preheated basement.

Thermal modeling shows that the early intrusion of relatively thin sills may lead to a thorough preheating of cold basement to temperatures of ca. 350 °C. Subsequent intrusions can then cause partial melting of the latter to produce the abundant pegmatite, which would not have been feasible without preheating the basement.

Comparison of Nittis with the Finnish Portimo and Penikat intrusions

The Paleoproterozoic Portimo Complex in northern Finland is not only broadly coeval with the Monchegorsk Complex, but it also hosts several sizable examples of contact-style sulfide mineralization related to the basal contact of the intrusion (e.g., Iljina, 1994).

The Suhanko-Konttijärvi intrusion in the southern part of the Portimo Complex includes a succession of orthopyroxene-rich cumulates in its lower portion (e.g., Ahmavaara), which reaches up to 150 m in thickness with abundant floor rock xenoliths (Iljina 1992). However, the modal proportion of plagioclase is much higher at this stratigraphic level compared to the Nittis intrusion. Another important stratigraphic difference is the presence of a relatively thick marginal zone at Portimo. This zone is entirely missing at Nittis and Nyud, the latter being characterized by a relatively thin basal contaminated zone of approximately 20 m, comprising tonalite and pegmatite that give way to melanorite. The basal portion of the Narkaus intrusion in the northern part of the Portimo Complex consists of an about 80-m-thick

orthopyroxenite, similar to Nittis, but it also hosts a massive chromite layer, which does not occur at Nittis. Therefore, a direct correlation with Paleoproterozoic Finnish intrusions proves to be inexpedient. In fact, the orthopyroxenitic body at Nittis is much thicker than in any of the Finnish intrusions, which suggests that the total volume of magma may have been significantly larger in the Monchegorsk Complex.

Another richly mineralized Paleoproterozoic intrusion in northern Finland is the Penikat intrusion, hosting at least seven PGE-enriched horizons (Alapieti and Halkoaho, 1995). Notably, most samples from Penikat are characterized by relatively strong negative Nb-Ta anomalies similar to the Monchegorsk Complex (Maier et al., in review); however, the exceptionally primitive SJ Reef at Penikat as well as the most primitive ophitic orthopyroxenite from Nittis lack this feature (Fig. 10 B), which may indicate that the parental magma to the most primitive rocks at both intrusions may not have necessarily featured a negative Nb-Ta anomaly. This is particularly important with respect to magma derivation as negative Nb-Ta anomalies are consistent with either melting of asthenospheric mantle followed by crustal contamination or melting of the sub-continental lithospheric mantle (SCLM) (e.g., Amelin and Semenov, 1996; Hanski et al., 2001b; Huhma et al., 1990; Puchtel et al., 1997; Yang et al., 2016). Since both alternatives have been considered as a possible source for the 2.5 to 2.44 Ga magmatism across the Fennoscandian Shield, the lack of negative Nb-Ta anomalies in some of the most primitive lithologies from the Monchegorsk Complex and the Penikat intrusion suggests that the widespread Nb-Ta depletion may not be a primary feature, inherited from the source region, but resulted from crustal contamination of asthenospheric mantle melt. This model would be consistent with recent Os, Nd, and Sr isotope data from Yang et al. (2016), which also argue for a mantle plume rather than an SCLM source.

Origin of cross-cutting massive sulfide veins

The ubiquitous cross-cutting massive sulfide veins associated with the NKT Massif seem to postdate the solidification of the host cumulates based on the sharp contact relationships between the two. Detailed element mapping of the vein contact reveals a 1 to 2-mm-thick alteration halo, with localized sulfide infiltration into the host rock, possibly reflecting small-scale partial melting (Fig. 6 D). Mantle-normalized chalcophile element patterns also suggest a different origin of these veins in comparison to the interstitial sulfide mineralization concentrated at the basal contact of the intrusion (Fig. 14 G, H). The extremely high Pd/Ir ratios of up to 15,000 strongly resemble Cu-rich veins at Noril'sk, Cape Smith, Sudbury and PGE-rich sulfide veins at Kilvenjärvi (Portimo Complex), representing highly fractionated sulfide liquid (e.g., Andersen et al., 2006; Barnes and Lightfoot, 2005; Duran et al., in press; Li et al., 1992). Modeling of sulfide segregation from an undepleted picrite at different R factors together with variable degrees of sulfide liquid fractionation provides further insight into the formation and origin of these veins.

Our chalcophile element data indicate that the veins represent highly fractionated sulfide liquid (melt fraction F ~ 10 %) at different R factors, ranging from less than 100 to more than 100,000 (Fig. 16). Furthermore, massive sulfide mineralization associated with micronorites cross-cutting the Nyud intrusion has largely similar chalcophile element pattern that lack the positive Rh anomaly typical of interstitial sulfide mineralization in the mafic-ultramafic cumulates of the Monchegorsk Complex (Fig. 14 G). Hence, these sulfide veins do not seem to be directly related to the formation of the contact-style PGE-Ni-Cu mineralization intersected at the base of Nittis and Nyud.

Note on the Dunite Block and its relation to the Monchegorsk Complex

The Dunite Block is generally considered to be a tectonically uplifted ultramafic block, which represents the lowermost portion of the Monchegorsk Complex (e.g., Chistyakova et al., 2015; Smolkin et al., 2004). It hosts the most primitive lithologies in the Monchegorsk area dominated by dunite and lherzolite with highly magnesian olivine, reaching forsterite contents of up to 91.6 mol %. Subsolidus re-equilibration between olivine and chromite, however, may have affected olivine compositions to a certain degree, even though analyses were primarily conducted on olivine cores (e.g., Ozawa, 1984). The corresponding parental magma would have most likely been a liquid of komatiitic composition with Mg# ~ 77, possibly similar to broadly coeval komatiites from the Central Lapland Greenstone Belt described by Hanski et al. (2001a). As a consequence, the SHMB, considered to be the parental magma for most Paleoproterozoic layered intrusions in the Fennoscandian Shield, including the NKT Massif, would have merely represented a fractionation product of a komatiite. Alternatively, the Dunite Block crystallized from a distinct batch of magma, but the close temporal and spatial relationship between the Dunite Block and the other parts of the Monchepluton strongly suggests a common origin.

Another important difference between the Dunite Block and the NKT Massif is the mineral chemistry of the ultramafic cumulates: orthopyroxene from the Dunite Block has considerably lower Cr concentrations than orthopyroxene from Travyanaya (3000 ppm vs. 5000 ppm Cr) at similar Mg# (Fig. 8); the latter being inconsistent with fractional crystallization of a komatiitic parental magma. However, Cr concentrations of orthopyroxene are not only controlled by the parental magma composition, but also by the oxygen fugacity, as magma oxidation results in a higher partition coefficient for Cr between orthopyroxene and melt (Barnes, 1986b). In addition, all NKT Massif

lithologies are saturated in sulfide, whereas none of the analyzed Dunite Block samples contain cumulus sulfide.

These characteristics can only be explained, if sulfide saturation occurred after the crystallization of the cumulus minerals that were later emplaced as the Dunite Block. Therefore, it is likely that highly magnesian cumulus phases were crystallizing from a sulfide-undersaturated magma, while it was undergoing progressive contamination with basement lithologies. This eventually led to sulfide saturation along with an increase in the oxygen fugacity of the magma, which increased the partition coefficient for Cr between orthopyroxene and melt, and produced Cr-rich orthopyroxene. Subsequently, the overlying portions of the complex crystallized from a sulfide-saturated magma. The model, however, implies that the SHMB only represents a fractionation product of a contaminated komatiitic parental magma. Ultimately, the Dunite Block, as an early magmatic phase, may have also contributed to the preheating of the basement, thus facilitating the formation of contact-style mineralization.

Summary and implications for exploration

Our study highlights key processes that lead to the formation of contact-style sulfide mineralization, based on the geology and geochemistry of the Monchegorsk Complex. The chalcophile element chemistry indicates that sulfide saturation occurred relatively early, possibly in a staging chamber, prior to the final emplacement of the complex as all lithologies contain cumulus sulfide. Therefore, the critical control on the formation of a sizable deposit is the efficient collection of sulfide in distinct zones of a layered intrusion, i. e. along the basal intrusion contact.

The frequent brecciation of mafic-ultramafic rocks, basement lithologies and felsic pegmatite, especially in the contact zone of the intrusion, suggests a multi-stage

emplacement of the complex. Our thermal modeling shows that the early intrusion of sills may lead to a thorough preheating of the cold basement to temperatures of ca. 350 °C.

The basement preheating did not only facilitate the assimilation of (S-rich) basement lithologies to trigger sulfide saturation, but it also affected cooling rates, which directly controlled the duration of potential sulfide accumulation through gravitational settling, especially in the center of the intrusion, where permeability was maintained the longest due to slower cooling relative to more peripheral parts. Moreover, dehydration melting of the basement introduced water and carbon dioxide into the magma, resulting in local melting of cumulus phases, which increased the porosity of the cumulate or crystal mush towards the base. This interstitial space was then filled with sulfide liquid. In addition, the volatiles may have also reduced the viscosity of the interstitial melt, facilitating sulfide settling. The lack of preheating, however, considerably reduces the degree and extent of potential interaction between the magma and the basement, which leads to an inefficient collection of sulfide liquid at the base of the complex.

As a consequence, layered intrusions, comprising two or more temporally related, but distinct injections or pulses of magma, should be prospective with respect to contact-style sulfide mineralization. Notably, the richest contact-style PGE deposits in the northern limb of the Bushveld Complex are located in areas where the Lower Zone is present (see McDonald et al., 2017 for a detailed geological map of the northern limb); the same applies to the Portimo Complex, where the presence of earlier Portimo Dykes seems to correlate with higher grade mineralization (see Iljina and Lee, 2005). Moreover, Groshev et al. (2009) suggested that the 300-m-thick mineral-

ized zone at the base of the Fedorova intrusion was emplaced after the formation of the more than 4-km-thick mafic-ultramafic main body of the layered intrusion.

Acknowledgments

We thank Anthony Oldroyd and Duncan Muir for their help with sample preparation and analytical work. The manuscript benefited from constructive reviews by Marco Fiorentini and Alexey Ariskin. We also thank Larry Meinert for editorial handling. BTK is particularly grateful for fieldwork support provided by the Society of Economic Geologists Foundation (SEGF) and the Mineralogical Society of Great Britain and Ireland. Special thanks go to Eurasia Mining and JSC Central Kola Expedition, in particular to Oleg Kazanov, for providing access to drill core. The project was supported by funds from the Canada Research Chair of S.-J. Barnes and the Russian Foundation for Basic Research (grant No. 15-35-20501).

Captions

Fig. 1. Simplified geological map of the north-eastern part of the Fennoscandian Shield, showing the location of Paleoproterozoic layered intrusions. Modified after Alapieti et al. (1990).

Fig. 2. Simplified geological map of the Monchegorsk Complex. The location of diamond drill cores used in this study are shown as red circles. Solid and dashed red lines indicate Ni-Cu-PGE mineralization. The inset shows the full extent of the Monchegorsk Complex, which is composed of the crescent-shaped Monchepluton (dark gray) and the elongated Main Ridge (light gray). 1: Volchetundra; 2: Monchetundra; 3: Chunatundra. Abbreviations: per = peridotite; px = pyroxenite; chr = chromite.

Fig. 3. Simplified stratigraphic column across the Monchepluton together with the Mg# of orthopyroxene from the Dunite Block, the NKT Massif and Nyud (this study).

Red circles show outcrop samples, whereas black circles represent drill core samples. Abbreviations: interlay. = interlayered; px = pyroxenite; per = peridotite.

Fig. 4. Typical lithologies from the ultramafic Nittis intrusion. (A, B) Mineralized contact zone between ophitic orthopyroxenite and the underlying basement lithologies with a ca. 2-m-thick interval of mineralized metasediment. Note the complex interlayering between metasediment and pegmatite (drill hole MT79: 146.5 - 153.2 m depth). (C) Layered orthopyroxenite with abundant mm-sized sulfide veins (MT79: 120.8 m depth), overlying finely disseminated interstitial sulfide mineralization (MT79: 121.6 m depth). (D) Dark sub-mm-thick PGE-rich sulfide vein in layered orthopyroxenite. Note that this sample contains ~ 30 ppm Pt + Pd (sample 79-39). (E) Steeply dipping massive Ni-Cu sulfide vein hosted by orthopyroxenite close to the center of the Nittis intrusion. Abbreviations: opx = orthopyroxenite.

Fig. 5. Schematic geological cross-sections, corresponding to profiles A-B (NKT Massif), C-D (Nittis), E-F (Nyud) in Figure 2. Red lines indicate vertical massive sulfide veins. Modified from Chashchin and Mitrofanov (2014) and Dokuchaeva and Yakovlev (1994).

Fig. 6. Elemental maps of different types of sulfide mineralization associated with the NKT Massif. (A) Thin sulfide veinlets cross-cutting harzburgite from Travyanaya (sample 15TMAS-5). (B) Interstitial sulfide mineralization in orthopyroxenite from the basal contact zone at Nittis (sample 79-138). (C) Interstitial sulfide in ophitic gabbronorite from the base of Travyanaya (sample 15TMAS-1). (D) Contact between olivine-orthopyroxenite and vein-hosted massive sulfide mineralization from the central part of the Nittis intrusion (sample 15NMAS-1). Note the local injection of sulfide into the immediate host rock. Abbreviations: opx = orthopyroxene; pl = plagioclase; amph = amphibole; chr = chromite; sul = sulfide; cpy = chalcopyrite; pn = pentlandite; po = pyrrhotite.

Fig. 7. Photomicrographs of major rock types in the Nittis and Nyud intrusions. (A) Strongly layered orthopyroxenite from Nittis; crossed polarized light (XPL) (sample 94-118). (B) Melanorite from Nyud; XPL (sample 1815-11). (C) Pegmatite from the

contact zone at Nittis; XPL (sample 79-150). (D) Xenolith of banded mica schist from the contact zone at Nittis; plane polarized light (sample 79-156).

Fig. 8. Plot of Cr concentrations vs. Mg# in orthopyroxene from the Dunite Block, the NKT Massif and the Nyud intrusion.

Fig. 9. Lithophile element variation of lithologies from the Dunite Block, the NKT Massif and the Nyud intrusion. (A) CaO vs. MgO. (B) Al_2O_3 vs. MgO + Fe_2O_3. (C) Cr vs. MgO. (D) Cr/V vs. Mg#. Data from the Fedorova intrusion were taken from Schissel et al. (2002). Abbreviations: ol = olivine; opx = orthopyroxene; cpx = clinopyroxene; pl = plagioclase; chr = chromite.

Fig. 10. Primitive mantle-normalized multi-element variation diagram of Monchegorsk lithologies analyzed for this study. Normalization values were taken from McDonough and Sun (1995). Data for the siliceous high-Mg basalts (SHMB) and the SJ Reef were taken from Guo et al. (2013) and Maier et al. (in review), respectively.

Fig. 11. Compositional variation of lithophile elements and orthopyroxene compositions across the Nittis intrusion. Note that orthopyroxene from the mineralized orthopyroxenite has slightly higher Mg# due to subsolidus re-equilibration with sulfide.

Fig. 12. Binary variation diagram of chalcophile elements. (A) Ni vs. S. (B) Cu vs. S. (C) Pt vs. S. (D) Pd vs. S. (E) Ir vs. S. (F) Cu/S vs. S. (G) Pt/S vs. S. (H) Pd vs. Pt. (I) Ir vs. Pd. (J) Pd/Pt vs. Pd/Ir. (K) Pd/Rh vs. S. Note that sulfide veins plot in a distinct field away from the samples containing interstitial sulfide.

Fig. 13. Downhole chalcophile element geochemistry for drill holes, intersecting the basal mineralized contact at (A) Nittis and (B) Nyud. The primitive mantle value was taken from Barnes and Maier (1999).

Fig. 14. Primitive mantle-normalized chalcophile element pattern of lithologies from the Dunite Block, the NKT Massif and the Nyud intrusion. (A) Dunite Block. (B)

Travyanaya. (C) Kumuzhya. (D) Nittis. (E) Nyud. (F) Basement lithologies. (G) Sulfide veins at Travyanaya. (H) Sulfide veins at Nittis. Abbreviations: gn = gabbronorite; opx = orthopyroxenite; hz = harzburgite; min = mineralized; ol = olivine. Data for the Portimo Complex and the Fedorova intrusion were taken from Iljina et al. (1992) and Groshev et al. (unpublished data), respectively. Normalization factors were taken from Barnes and Maier (1999).

Fig. 15. Schematic model for the formation of contact-style sulfide mineralization in the Monchegorsk Complex. Note that the partial melting of the basement in (C) relies on the preheating of the basement through the intrusion of early sills and dykes. See text for explanation.

Fig. 16. Binary ratio plot of Ni/Pd vs. Cu/Ir. The black solid line shows model sulfide compositions at different R factors. The black dashed lines represent model compositions of monosulfide solid solution (mss), crystallizing from sulfide liquids undergoing fractionation, and residual liquid. The dotted lines show different end-member mss (blue) and residual sulfide liquid (red) compositions, assuming different degrees of fractionation (F = fraction of residual liquid). Sulfide melt/silicate melt D values: 30,000 for the PGE, 1,000 for Cu and 500 for Ni. Mss/sulfide melt D values as summarized in Maier and Barnes (1999). Half-filled symbols represent samples, containing vein-hosted sulfide.

Fig. 17. Temperature-depth profile for different modeled intrusion emplacement scenarios. (A) Preheating of the basement by multiple sills with a thickness of 50 m and a spacing of 250 m. (B) Emplacement of a 1.5-km-thick crystal mush into preheated basement at a depth of 2.5 km. (C) Emplacement of a 1.5-km-thick crystal mush at a depth of 2.5 km into cold basement. Note that significant partial melting of the basement (> 700 °C) is only feasible in a preheated basement. See text and Electronic Appendix 1 for further explanation. Green = mafic-ultramafic rocks; pink = basement.

Fig. A1. Lithological logs for drill cores MT79 and 1815, intersecting the basal intrusion contact at Nittis and Nyud, respectively.

Fig. A2. Elemental map of orthopyroxenite sample 79-23. Abbreviations: opx = orthopyroxene; cpx = clinopyroxene; sul = sulfide.

Table 1. Comparison of results obtained at LabMaTer and the accepted values for international standards

Table A1. Mineral chemistry

Table A2. Whole rock geochemical analyses

Electronic Appendix 1: Derivation of the one-dimensional explicit heat function.

References

Alapieti, T.T., 1982, The Koillismaa layered igneous complex, Finland: Its structure, mineralogy and geochemistry, with emphasis on the distribution of chromium: Bulletin of Geological Survey of Finland, v. 319, 116 p.

Alapieti, T.T., Filen, B.A., Lahtinen, J.J., Lavrov, M.M., Smolkin, V.F., and Voitsekhovsky, S.N., 1990, Early Proterozoic layered intrusions in the northeastern part of the Fennoscandian Shield: Mineralogy and Petrology, v. 42, p. 1–22.

Alapieti, T.T., and Halkoaho, T.A.A., 1986, Cryptic variation of augite in the Penikat layered intrusion, northern Finland, with reference to megacyclic units and PGE-enriched zones. Mineralogy and Petrology, v. 54, p. 11–24.

Alapieti, T.T., and Lahtinen, J.J., 1986, Stratigraphy, petrology, and platinum-group element mineralization of the early Proterozoic Penikat layered intrusion, northern Finland: Economic Geology, v. 81, p. 1126–1136.

Amelin, Y.V., Heaman, L.M., and Semenov, V.S., 1995, U-Pb geochronology of layered mafic intrusions in the eastern Baltic Shield: implications for the timing and duration of Paleoproterozoic continental rifting: Precambrian Research, v. 75, p. 31–46.

Amelin, Y.V., and Semenov, V.S., 1996, Nd and Sr isotopic geochemistry of mafic layered intrusions in the eastern Baltic shield: implications for the evolution of Paleoproterozoic continental mafic magmas: Contributions to Mineralogy and Petrology, v. 124, p. 255–272.

Andersen, J.C.Ø., Thalhammer, O.A.R., and Schoenberg, R., 2006, Platinum-group element and Re-Os isotope variations of the high-grade Kilvenjärvi platinum-group element deposit, Portimo Layered Igneous Complex, Finland: Economic Geology, v. 101, p. 159–177.

Balashov, Y.A., Bayanova, T.B., and Mitrofanov, F.P., 1993, Isotope data on the age and genesis of layered basic-ultrabasic intrusions in the Kola Peninsula and northern Karelia, northeastern Baltic Shield: Precambrian Research, v. 64, p. 197–205.

Barnes, S.J., 1986a, The effect of trapped liquid crystallization on cumulus mineral compositions in layered intrusions: Contributions to Mineralogy and Petrology, v. 93, p. 524–531.

Barnes, S.J., 1986b, The distribution of chromium among orthopyroxene, spinel and silicate liquid at atmospheric pressure: Geochimica et Cosmochimica Acta, v. 50, p. 1889–1909.

Barnes, S.-J., and Francis, D., 1995, The distribution of platinum-group elements, nickel, copper, and gold in the Muskox layered intrusion, Northwest Territories, Canada: Economic Geology, v. 90, p. 135–154.

Barnes, S.-J., and Lightfoot, P.C., 2005, Formation of magmatic nickel sulfide ore deposits and processes affecting their copper and platinum group element contents, in Hedenquist, J.W., Thompson, J.F.H., Goldfarb, R.J., and Richards, J.P., eds., Economic Geology 100th Anniversary Volume, p. 179–213.

Barnes, S.-J., and Maier, W.D., 1999, The fractionation of Ni, Cu and the noble metals in silicate and sulfide liquids, in Keays, R.R., Lesher, C.M., Lightfoot, P.C., and Farrow, C.E.G., eds., Dynamic processes in magmatic ore deposits and their application in mineral exploration, Short Course Volume 13, p. 69–106.

Barnes, S.-J., Melezhik, V.A., and Sokolov, S.V., 2001, The composition and mode of formation of the Pechenga nickel deposits, Kola Peninsula, northwestern Russia: Canadian Mineralogist, v. 39, p. 447–471.

Bayanova, T.B., Nerovich, L.I., Mitrofanov, F.P., Zhavkov, V.A., and Serov, P.A., 2010, The Monchetundra Basic Massif of the Kola region: New geological and isotope geochronological data: Doklady Earth Sciences, v. 431, p. 288–293.

Bédard, L.P., Savard, D., and Barnes, S.-J., 2008, Total sulfur concentration in geological reference materials by elemental infrared analyser: Geostandards and Geoanalytical Research, v. 32, p. 203–208.

Bekker, A., Grokhovskaya, T.L., Hiebert, R., Sharkov, E.V., Bui, T.H., Stadnek, K.R., Chashchin, V.V., and Wing, B.A., 2016, Multiple sulfur isotope and mineralogical constraints on the genesis of Ni-Cu-PGE magmatic sulfide mineralization of the Monchegorsk Igneous Complex, Kola Peninsula, Russia: Mineralium Deposita, v. 51, p. 1035–1053.

Bleeker, W., and Ernst, R.E., 2006, Short-lived mantle generated magmatic events and their dyke swarms: the key unlocking Earth's paleogeographic record back to 2.6 Ga, in Hanski, E.J., Mertanen, S., Rämö, O.T., and Vuollo, J.I., eds., Dyke Swarms - Time Markers of Crustal Evolution: London, Taylor and Francis, p. 3–26.

Buchanan, D.L., Nolan, J., Suddaby, P., Rouse, J.E., Viljoen, M.J., and Davenport, J.W.J., 1981, The genesis of sulfide mineralization in a portion of the Potgietersrus Limb of the Bushveld Complex: Economic Geology, v. 76, p. 568–579.

Campbell, I.H., 1978, Some problems with the cumulus theory: Lithos, v. 11, p. 311–323.

Capobianco, C.J., and Drake, M.J., 1990, Partitioning of ruthenium, rhodium, and palladium between spinel and silicate melt and implications for platinum group element fractionation trends: Geochimica et Cosmochimica Acta, v. 54, p. 869–874.

Cawthorn, R.G., and Meyer, F.M., 1993, Petrochemistry of the Okiep copper district basic intrusive bodies, northwestern Cape Province, South Africa: Economic Geology, v. 88, p. 590–605.

Chashchin, V.V., Galkin, A.S., Ozeryanskii, V.V., and Dedyukhin, A.N., 1999, Sopcha lake chromite deposit and its platinum potential, Monchegorsk pluton, Kola Peninsula (Russia): Geology of Ore Deposits, v. 41, p. 460–468.

Chistyakova, S., Latypov, R., and Zaccarini, F., 2015, Chromitite dykes in the Monchegorsk Layered Intrusion, Russia: In situ crystallization from chromite-saturated magma flowing in conduits: Journal of Petrology, v. 56, p. 2395–2424.

Ciborowski, T.J.R., Kerr, A.C., Ernst, R.E., McDonald, I., Minifie, M.J., Harlan, S.S., and Millar, I.L., 2015, The Early Proterozoic Matachewan Large Igneous Province: Geochemistry, petrogenesis, and implications for earth evolution: Journal of Petrology, v. 56, p. 1459–1494.

Dedeev, A.V., Khashkovskaya, T.N., and Galkin, A.S., 2002, PGE mineralization of the Monchegorsk layered mafic–ultramafic intrusion of the Kola Peninsula, in Cabri, L.J., ed., The geology, geochemistry, mineralogy and mineral beneficiation of platinum-group elements (CIM Special Volume 54): Montreal, p. 569–577.

Duran, C.J., Barnes, S.-J., Pleše, P., Kudrna Prašek, M., Zientek, M.L., and Pagé, P., in press, Fractional crystallization-induced variations in sulfides from the Noril'sk-Talnakh mining district (polar Siberia, Russia): Ore Geology Reviews.

Eurasia Mining plc, 2010, Licence Extension and Drilling Update: News Announcement No. 0197Y (http://otp.investis.com/clients/uk/eurasia-mining/rns/regulatory-story.aspx?cid=403&newsid=249570).

Eurasia Mining plc, 2017, Russian Subsoil Agency Approves Maiden Reserves: News Announcement No. 6202G (http://otp.investis.com/clients/uk/eurasia-mining/rns/regulatory-story.aspx?cid=403&newsid=878255).

Fleet, M.E., Chryssoulis, S.L., Stone, W.E., and Weisener, C.G., 1993, Partitioning of platinum group elements and Au in the Fe-Ni-Cu-S system: Experiments on the fractional crystallization of sulphide melt: Contributions to Mineralogy and Petrology, v. 115, p. 36–44.

Gain, S.B., and Mostert, A.B., 1982, The geological setting of the platinoid and base metal sulfide mineralization in the Platreef of the Bushveld Complex in Drenthe, north of Potgietersrus: Economic Geology, v. 77, p. 1395–1404.

Godel, B., 2013, High-resolution X-ray computed tomography and its application to ore deposits: From data acquisition to quantitative three-dimensional measurements with case studies from Ni-Cu-PGE deposits: Economic Geology, v. 108, p. 2005–2019.

Groshev, N.Y., Nitkina, E.A., and Mitrofanov, F.P., 2009, Two-phase mechanism of the formation of platinum-metal basites of the Fedorova Tundra intrusion on the Kola Peninsula: New data on geology and isotope geochronology: Doklady Earth Sciences, v. 427, p. 1012–1016.

Guo, F., Maier, W.D., Vuollo, J.I., Lahaye, Y., Huhma, H., O'Brien, H., and Junttila, H., 2013, Geochemistry of the ~2.45 Ga mafic dykes in Northern Finland: constraints on the origin of PGE mineralization in coeval layered intrusions [ext. abs.]: SGA Biennial Meeting, 12th, Uppsala, Sweden, 2013, Extended Abstracts, p. 997–1000.

Hanski, E., Huhma, H., Rastas, P., and Kamenetsky, V.S., 2001a, The Palaeoproterozoic komatiite–picrite association of Finnish Lapland: Journal of Petrology, v. 42, p. 855–876.

Hanski, E., Walker, R.J., Huhma, H., and Suominen, I., 2001b, The Os and Nd isotopic systematics of c. 2.44 Ga Akanvaara and Koitelainen mafic layered intrusions in northern Finland: Precambrian Research, v. 109, p. 73–102.

Hölttä, P., Balagansky, V., Garde, A.A., Mertanen, S., Peltonen, P., Slabunov, A., Sorjonen-Ward, P., and Whitehouse, M., 2008, Archean of Greenland and Fennoscandia: Episodes, v. 31, p. 13–19.

Holwell, D.A., Keays, R.R., Firth, E.A., and Findlay, J., 2014, Geochemistry and mineralogy of platinum group element mineralization in the River Valley Intrusion, Ontario, Canada: A model for early-stage sulfur saturation and multistage emplacement and the implications for "contact-type" Ni-Cu-PGE sulfide mineralization: Economic Geology, v. 109, p. 689–712.

Huhma, H., Cliff, R.A., Perttunen, V., and Sakko, M., 1990, Sm-Nd and Pb isotopic study of mafic rocks associated with early Proterozoic continental rifting: the Peröpohja schist belt in northern Finland: Contributions to Mineralogy and Petrology, v. 104, p. 369–379.

Huhtelin, T., 2015, The Kemi chromite deposit, in Maier, W.D., Lahtinen, R., O'Brien, H., eds., Mineral Deposits of Finland: Amsterdam, Elsevier, p. 165–178.

Huppert, H.E., Stephen, R., and Sparks, J., 1985, Cooling and contamination of mafic and ultramafic magmas during ascent through continental crust: Earth and Planetary Science Letters, v. 74, p. 371–386.

Iljina, M., 1994, The Portimo layered igneous complex with emphasis on diverse sulphide and platinum-group element deposits: Ph.D. thesis, Oulu, University of Oulu, 158 p.

Iljina, M.J., Alapieti, T.T., and McElduff, B.M., 1992, Platinum-group element mineralization in the Suhanko-Konttijärvi intrusion, Finland: Australian Journal of Earth Sciences, v. 39, p. 303–313.

Iljina, M.J., and Lee, C.A., 2005, PGE deposits in the marginal series of layered intrusions, in Mungall, J.E., ed., Exploration for platinum group element deposits: Oulu, Mineralogical Association of Canada Short Course Series Volume 35, 75–96.

James, R.S., Easton, R.M., Peck, D.C., and Hrominchuk, J.L., 2002, The East Bull Lake Intrusive Suite: Remnants of a ~ 2.48 Ga Large Igneous and Metallogenic Province in the Sudbury area of the Canadian Shield: Economic Geology, v. 97, p. 1577–1606.

Karykowski, B.T., Maier, W.D., Pripachkin, P.V., and Groshev, N.Y., 2016, The Monchegorsk Layered Complex – a natural laboratory for mineral deposit types associated with layered intrusions: Applied Earth Science, v. 125, p. 87–87.

Kinnaird, J.A., Hutchinson, D., Schurmann, L., Nex, P.A.M., and de Lange, R., 2005, Petrology and mineralisation of the southern Platreef: northern limb of the Bushveld Complex, South Africa: Mineralium Deposita, v. 40, p. 576–597.

Kozlov, E.K., 1973, Natural rock series of nickel-bearing intrusions and their metallogeny: Leningrad, Nauka, 288 p.

Latypov, R.M., 2003, The origin of marginal compositional reversals in basic-ultrabasic sills and layered intrusions by Soret fractionation: Journal of Petrology, v. 44, p. 1579–1618.

Lee, C.A., 1996, A review of mineralization in the Bushveld Complex and some other layered intrusions, in Cawthorn, R.G., ed., Developments in Petrology – Layered Intrusions: Amsterdam, Elsevier, p. 103–145.

Li, C., Naldrett, A.J., Coats, C.J.A., and Johannessen, P., 1992, Platinum, palladium, gold, copper-rich stringers at the Strathcona Mine, Sudbury; their enrichment by fractionation of a sulfide liquid: Economic Geology, v. 87, p. 1584–1598.

Lightfoot, P.C., Naldrett, A.J., and Hawkesworth, C.J., 1984, The geology and geochemistry of the Waterfall Gorge section of the Insizwa Complex with particular reference to the origin of the nickel sulfide deposits: Economic Geology, v. 79, p. 1857–1879.

Maier, W.D., and Barnes, S.-J., 1999, Platinum-group elements in silicate rocks of the Lower, Critical and Main zones at Union Section, western Bushveld Complex: Journal of Petrology, v. 40, p. 1647–1671.

Maier, W.D., and Barnes, S.J., 1996, Unusually high concentrations of magnetite at Caraiba and other Cu-sulfide deposits in the Curaca Valley, Bahia, Brazil: Canadian Mineralogist, v. 34, p. 717–731.

Maier, W.D., de Klerk, L., Blaine, J., Manyeruke, T., Barnes, S.-J., Stevens, M.V.A., and Mavrogenes, J.A., 2008, Petrogenesis of contact-style PGE mineralization in the northern lobe of the Bushveld Complex: comparison of data from the farms Rooipoort, Townlands, Drenthe and Nonnenwerth: Mineralium Deposita, v. 43, p. 255–280.

Maier, W.D., and Groves, D.I., 2011, Temporal and spatial controls on the formation of magmatic PGE and Ni–Cu deposits: Mineralium Deposita, v. 46, p. 841–857.

Maier, W.D., Määttää, S., Yang, S., Oberthür, T., Lahaye, Y., Huhma, H., and Barnes, S.-J., 2015, Composition of the ultramafic–mafic contact interval of the Great Dyke of Zimbabwe at Ngezi mine: Comparisons to the Bushveld Complex and implications for the origin of the PGE reefs: Lithos, v. 238, p. 207–222.

Manyeruke, T.D., Maier, W.D., and Barnes, S.-J., 2005, Major and trace element geochemistry of the Platreef on the farm Townlands, northern Bushveld Complex: South African Journal of Geology, v. 108, p. 381–396.

McDonald, I., Harmer, R.E., Holwell, D.A., Hughes, H.S.R., and Boyce, A.J., 2017, Cu-Ni-PGE mineralisation at the Aurora Project and potential for a new PGE province in the Northern Bushveld Main Zone: Ore Geology Reviews, v. 80, p. 1135–1159.

McDonald, I., and Holwell, D.A., 2011, Geology of the northern Bushveld Complex and the setting and genesis of the Platreef Ni-Cu-PGE deposit: Reviews in Economic Geology, v. 17, p. 297–327.

McDonald, I., and Viljoen, K.S., 2006, Platinum-group element geochemistry of mantle eclogites: a reconnaissance study of xenoliths from the Orapa kimberlite, Botswana: Applied Earth Science, v. 115, p. 81–93.

McDonough, W.F., and Sun, S. -s., 1995, The composition of the Earth: Chemical Geology, v. 120, p. 223–253.

Melezhik, V.A., and Sturt, B.A., 1994, General geology and evolutionary history of the Early Proterozoic Polmak-Pasvik-Pechenga-Imandra/Varzuga-Ust'Ponoy greenstone belt in the northeastern Baltic Shield: Earth-Science Reviews, v. 36, p. 205–241.

Mutanen, T., 1997, Geology and ore petrology of the Akanvaara and Koitelainen mafic layered intrusions and the Keivitsa-Satovaara layered complex, northern Finland: Bulletin of Geological Survey of Finland, v. 395, 233 p.

Ozawa, K., 1984, Olivine-spinel geospeedometry: Analysis of diffusion-controlled Mg-Fe^{2+} exchange: Geochimica et Cosmochimica Acta, v. 48, p. 2597–2611.

Page, N.J., 1979, Stillwater Complex, Montana: Structure, mineralogy, and petrology of the Basal Zone with emphasis on the occurrence of sulfides: U.S. Geological Survey Professional Paper 1038, 69 p.

Peck, D.C., Keays, R.R., James, R.S., Chubb, P.T., and Reeves, S.J., 2001, Controls on the formation of contact-type platinum-group element mineralization in the East Bull Lake intrusion: Economic Geology, v. 96, p. 559–581.

Puchtel, I.S., Haase, K.M., Hofmann, A.W., Chauvel, C., Kulikov, V.S., Garbe-Schönberg, C.-D., and Nemchin, A.A., 1997, Petrology and geochemistry of crustally contaminated komatiitic basalts from the Vetreny Belt, southeastern Baltic Shield: Evidence for an early Proterozoic mantle plume beneath rifted Archean continental lithosphere: Geochimica et Cosmochimica Acta, v. 61, p. 1205–1222.

Puchtel, I.S., and Humayun, M., 2001, Platinum group element fractionation in a komatiitic basalt lava lake: Geochimica et Cosmochimica Acta, v. 65, p. 2979–2993.

Roeder, P.L., and Emslie, R.F., 1970, Olivine-liquid equilibrium: Contributions to Mineralogy and Petrology, v. 29, p. 275–289.

Rundkvist, T.V., Bayanova, T.B., Sergeev, S.A., Pripachkin, P.V., and Grebnev, R.A., 2014, The Paleoproterozoic Vurechuaivench layered Pt-bearing pluton, Kola Peninsula: New results of the U-Pb (ID-TIMS, SHRIMP) dating of baddeleyite and zircon: Doklady Earth Sciences, v. 454, p. 1–6.

Rundqvist, D.V., and Mitrofanov, F.P., 1993, Precambrian Geology of the USSR: Amsterdam, Elsevier, 527 p.

Saini-Eidukat, B., Alapieti, T.T., Thalhammer, O.A.R., and Iljina, M.J., 1997, Siliceous, high-magnesian parental magma compositions of the PGE-rich Early Proterozoic layered intrusion belt of northern Finland, in Rongfu, P., ed., Proceedings of the 30th International Geological Congress: Utrecht, VSP, p. 177–197.

Savard, D., Barnes, S.-J., and Meisel, T., 2010, Comparison between nickel-sulfur fire assay Te co-precipitation and isotope dilution with high-pressure asher acid digestion for the determination of platinum-group elements, rhenium and gold: Geostandards and Geoanalytical Research, v. 34, p. 281–291.

Schissel, D., Tsvetkov, A.A., Mitrofanov, F.P., and Korchagin, A.U., 2002, Basal platinum-group element mineralization in the Federov Pansky layered mafic intrusion, Kola Peninsula, Russia: Economic Geology, v. 97, p. 1657–1677.

Serov, P.A., Nitkina, E.A., Bayanova, T.B., and Mitrofanov, F.P., 2007, Comparison of new U-Pb and Sm-Nd isotope data on rocks of the early barren phase and basal ore-bearing rocks in the PGE-bearing Fedorovo-Pana layered massif, Kola Peninsula: Doklady Earth Sciences, v. 416, p. 1125–1127.

Sharkov, E.V., and Chistyakov, A.V., 2012, The Early Paleoproterozoic Monchegorsk layered mafite-ultramafite massif in the Kola Peninsula: Geology, petrology, and ore potential: Petrology, v. 20, p. 607–639.

Singh, J., and Johannes, W., 1996, Dehydration melting of tonalites. Part I. Beginning of melting: Contributions to Mineralogy and Petrology, v. 125, p. 16–25.

Smolkin, V.F., Fedotov, Z.A., Orsoev, D.A., and Ohnenstetter, D., 2004, Ore-bearing layered Monchepluton, in Mitrofanov, F.P., and Smolkin, V.F., eds., Layered intrusions of the Monchegorsk ore region: petrology, mineralization, isotopy, deep structure: Apatity, KSC RAS, p. 36–75.

Vogel, D.C., Vuollo, J.I., Alapieti, T.T., and James, R.S., 1998, Tectonic, stratigraphic, and geochemical comparisons between ca. 2500–2440 Ma mafic igneous events in the Canadian and Fennoscandian Shields: Precambrian Research, v. 92, p. 89–116.

Vrevskii, A.B., Bogomolov, E.S., Zinger, T.F., and Sergeev, S.A., 2010, Polychronic sources and isotopic age of the volcanogenic complex (Arvarench Unit) of the Imandra-Varzuga structure, Kola Peninsula: Doklady Earth Sciences, v. 431, p. 386–389.

Yang, S.-H., Hanski, E., Li, C., Maier, W.D., Huhma, H., Mokrushin, A.V., Latypov, R., Lahaye, Y., O'Brien, H., and Qu, W.-J., 2016, Mantle source of the 2.44–2.50-Ga mantle plume-related magmatism in the Fennoscandian Shield: evidence from Os, Nd, and Sr isotope compositions of the Monchepluton and Kemi intrusions: Mineralium Deposita, v. 51, p. 1055–1073.

Zagorodny, V.G., Predovsky, A.A., Basalaev, A.A., Batieva, I.D., Borisov, A.Y., Vetrin, V.R., Voloshina, Z.M., Dokuchaeva, V.S., Zhangurov, A.A., and Kozlova, N.E., 1982, The Imandra-Varzuga Zone of the Karelides: Leningrad, Nauka, 280 p.

Zientek, M.L., 2012, Magmatic ore deposits in layered intrusions – Descriptive model for reef-type PGE and contact-type Cu-Ni-PGE deposits: U.S. Geological Survey Open-File Report 2012–1010, 48 p.

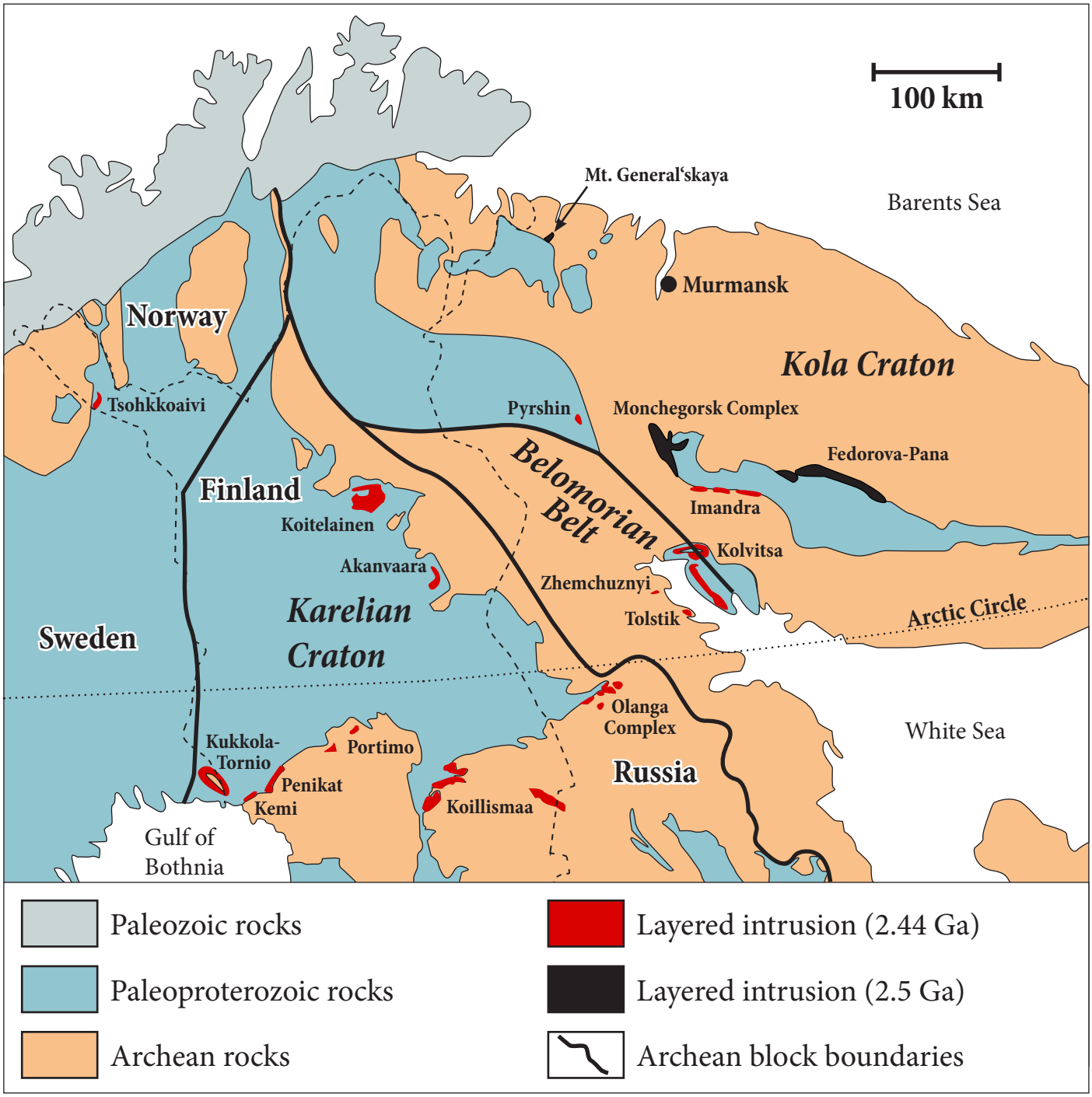
100 km
Mt. General'skaya
Barents Sea
Murmansk
Norway
Kola Craton
Tsohkkoaivi
Pyrshin
Monchegorsk Complex
Fedorova-Pana
Belomorian Belt
Finland
Imandra
Koitelainen
Kolvitsa
Akanvaara
Zhemchuznyi
Karelian Craton
Tolstik
Arctic Circle
Sweden
Olanga Complex
White Sea
Kukkola-Tornio
Portimo
Penikat
Kemi
Russia
Koillismaa
Gulf of Bothnia
Paleozoic rocks
Paleoproterozoic rocks
Archean rocks
Layered intrusion (2.44 Ga)
Layered intrusion (2.5 Ga)
Archean block boundaries

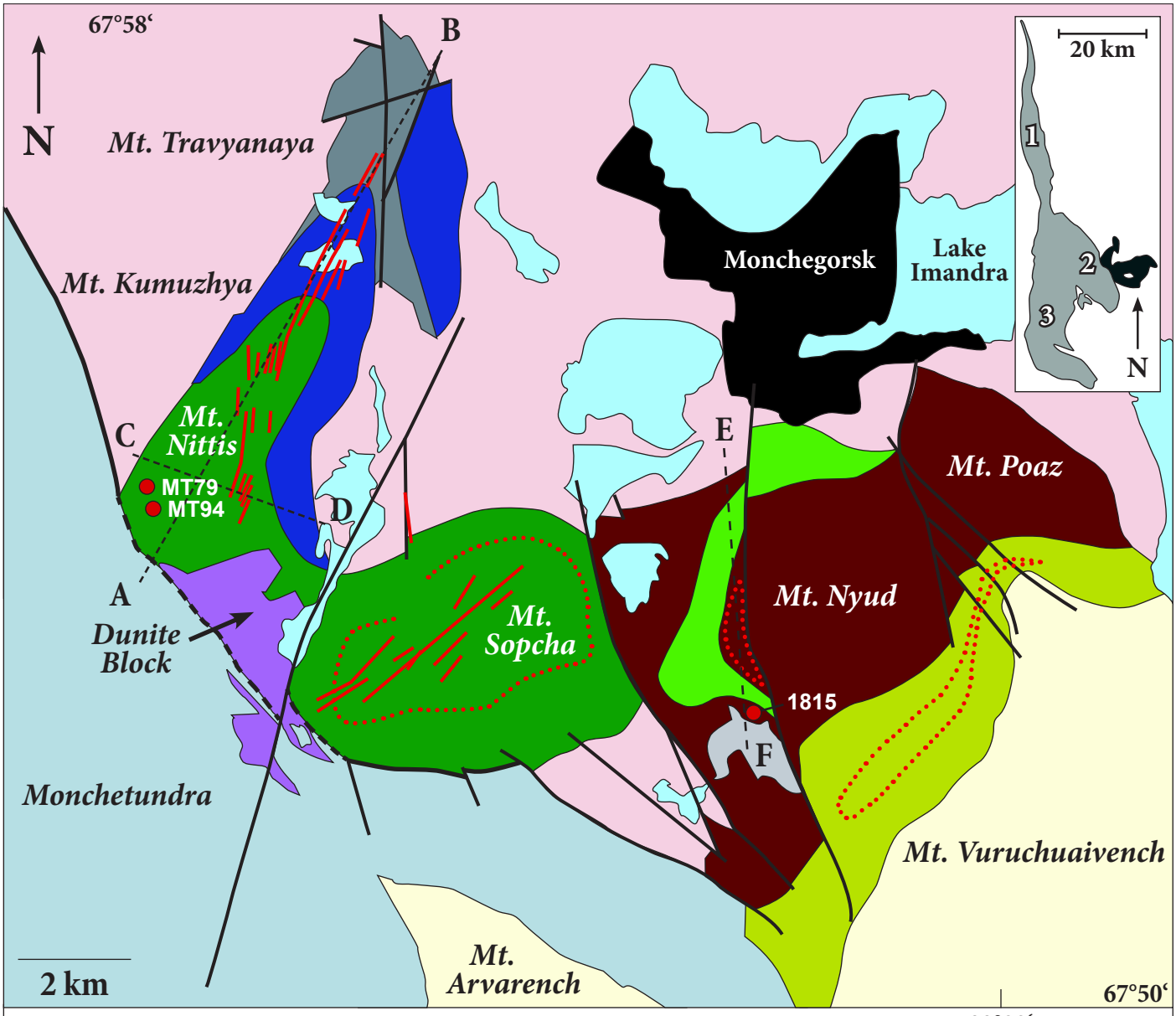

Monchepluton

- Gabbro (G-10)
- Norite
- Olivine-norite
- Orthopyroxenite
- Interlayered px-per
- Peridotite
- Chr-rich peridotite

Monchetundra

- Gabbro, gabbronorite, anorthosite

Vuruchuaivench

- Gabbro, gabbronorite, anorthosite

Other rocks types

- Volcano-sedimentary rocks (Imandra-Varzuga)
- Archean gneiss

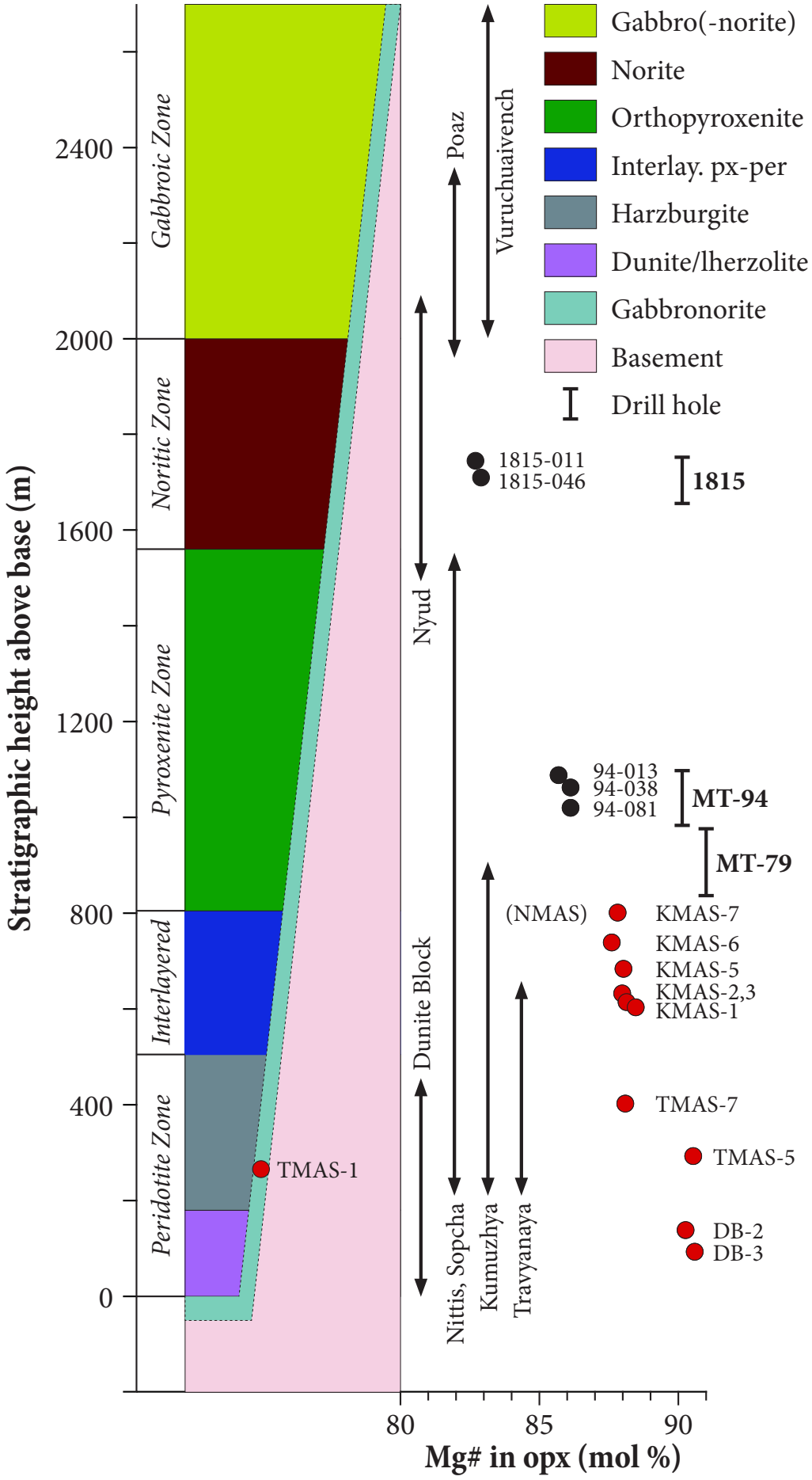
Stratigraphic height above base (m)
2400
2000
1600
1200
800
400
0
Gabbroic Zone
Noritic Zone
Pyroxenite Zone
Interlayered
Peridotite Zone
TMAS-1
Gabbro(-norite)
Norite
Orthopyroxenite
Interlay. px-per
Harzburgite
Dunite/lherzolite
Gabbronorite
Basement
Drill hole
Poaz
Vuruchuaivench
Nyud
Dunite Block
Nittis, Sopcha
Kumuzhya
Travyanaya
1815-011
1815-046
1815
94-013
94-038
94-081
MT-94
MT-79
(NMAS)
KMAS-7
KMAS-6
KMAS-5
KMAS-2,3
KMAS-1
TMAS-7
TMAS-5
DB-2
DB-3
80
85
90
Mg# in opx (mol %)

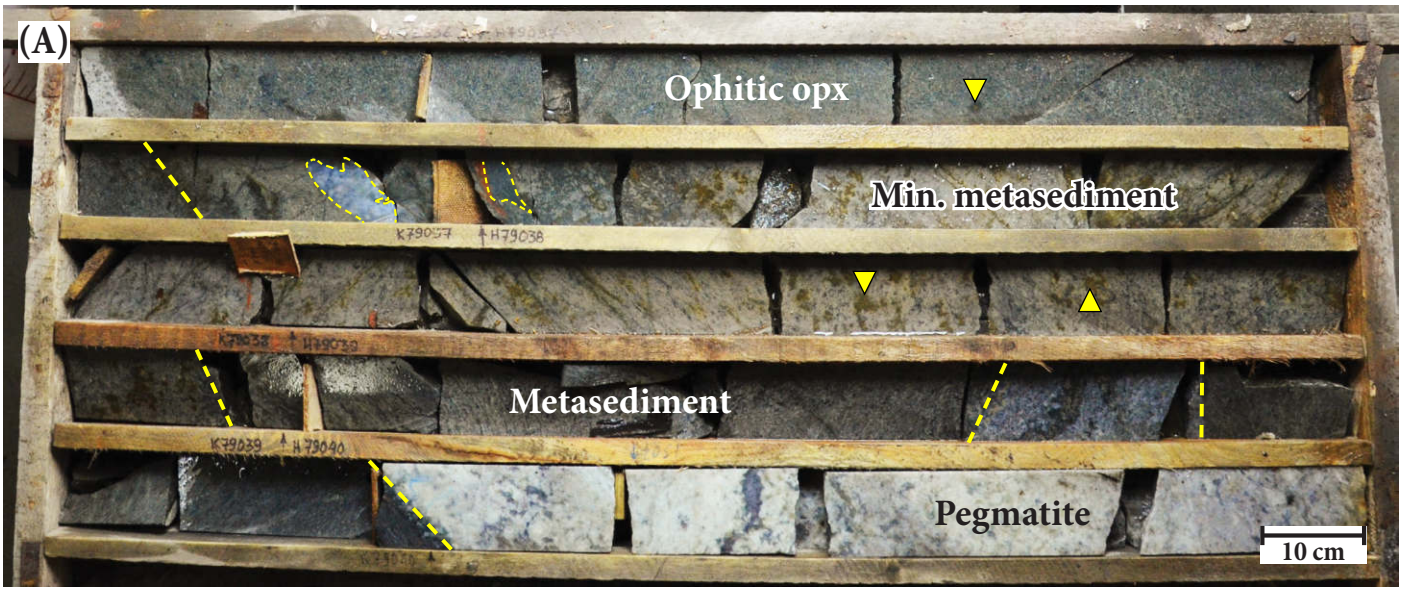
(A)
Ophitic opx
Min. metasediment
Metasediment
Pegmatite
10 cm

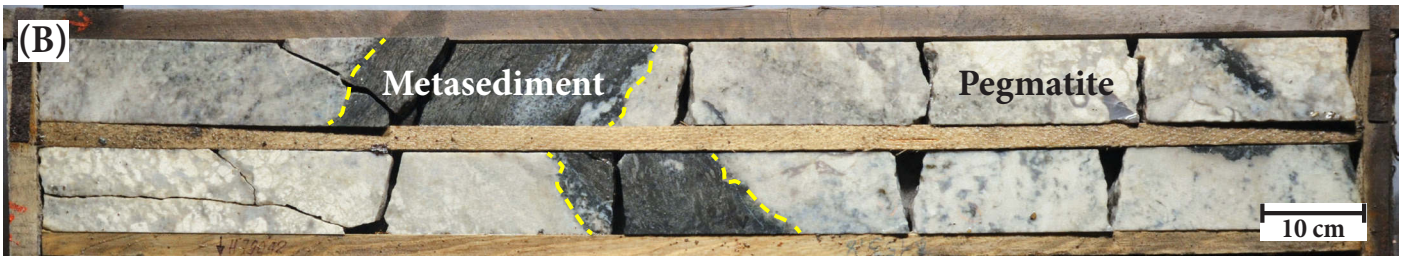
(B)
Metasediment
Pegmatite
10 cm


(C)
5 cm
Layered opx

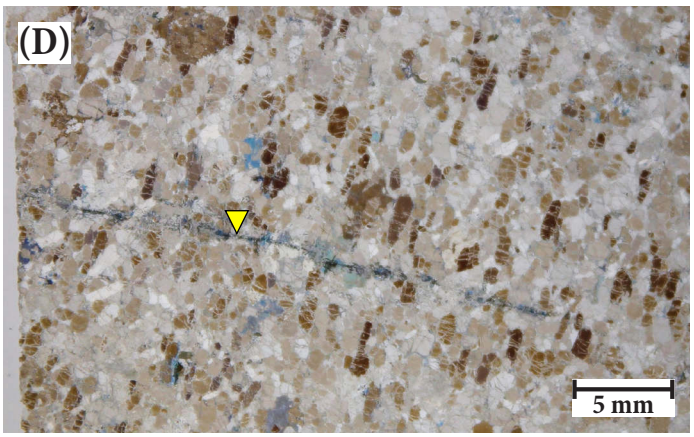
(D)
5 mm

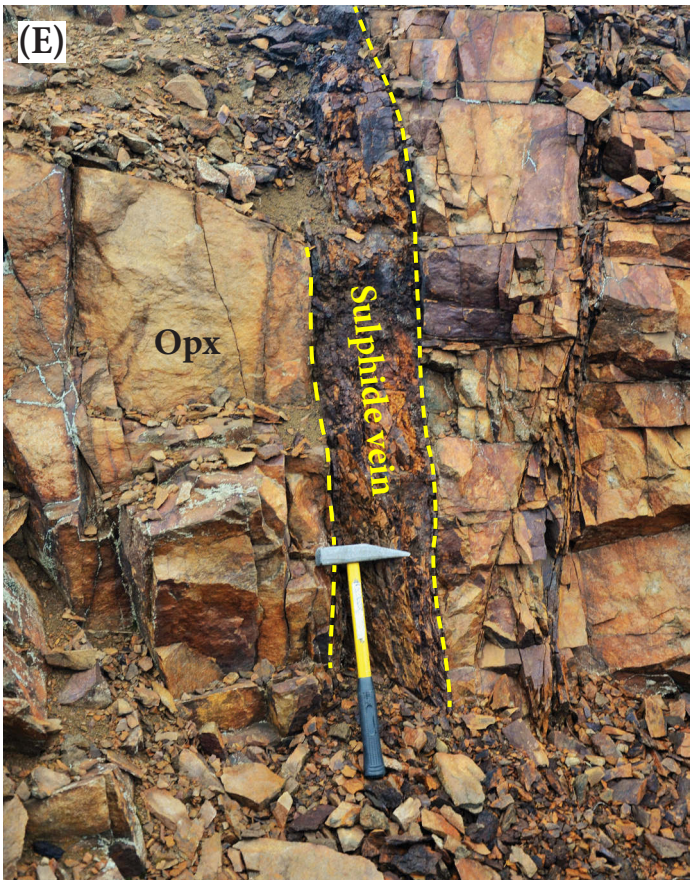
(E)
Opx
Sulphide vein

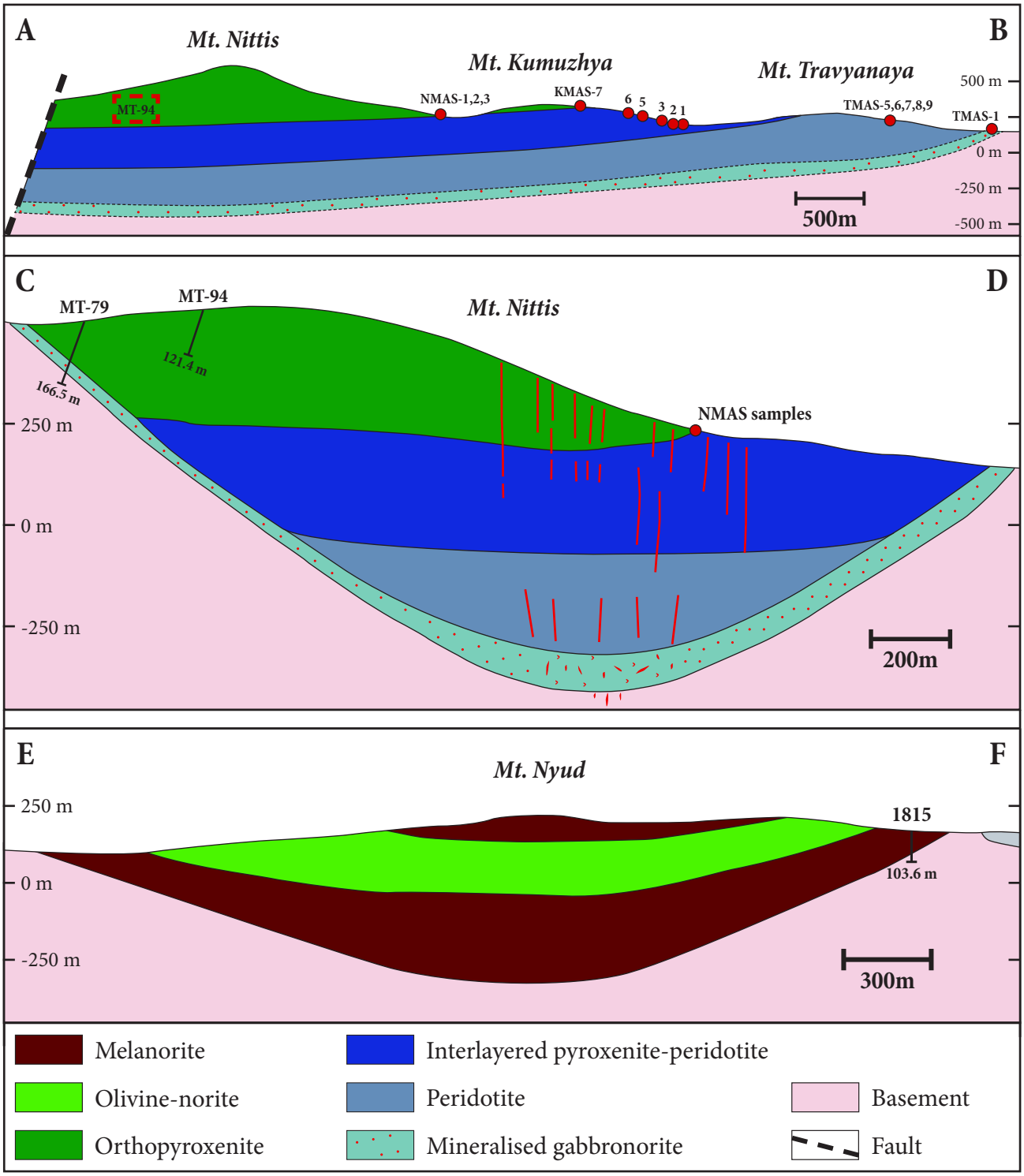
A
Mt. Nittis
Mt. Kumuzhya
Mt. Travyanaya
B
MT-94
NMAS-1,2,3
KMAS-7
6 5 3 2 1
TMAS-5,6,7,8,9
TMAS-1
500 m
0 m
-250 m
-500 m
500m
C
D
MT-79
MT-94
Mt. Nittis
121.4 m
166.5 m
NMAS samples
250 m
0 m
-250 m
200m
E
F
Mt. Nyud
250 m
1815
0 m
103.6 m
-250 m
300m
Melanorite
Olivine-norite
Orthopyroxenite
Interlayered pyroxenite-peridotite
Peridotite
Mineralised gabbronorite
Basement
Fault

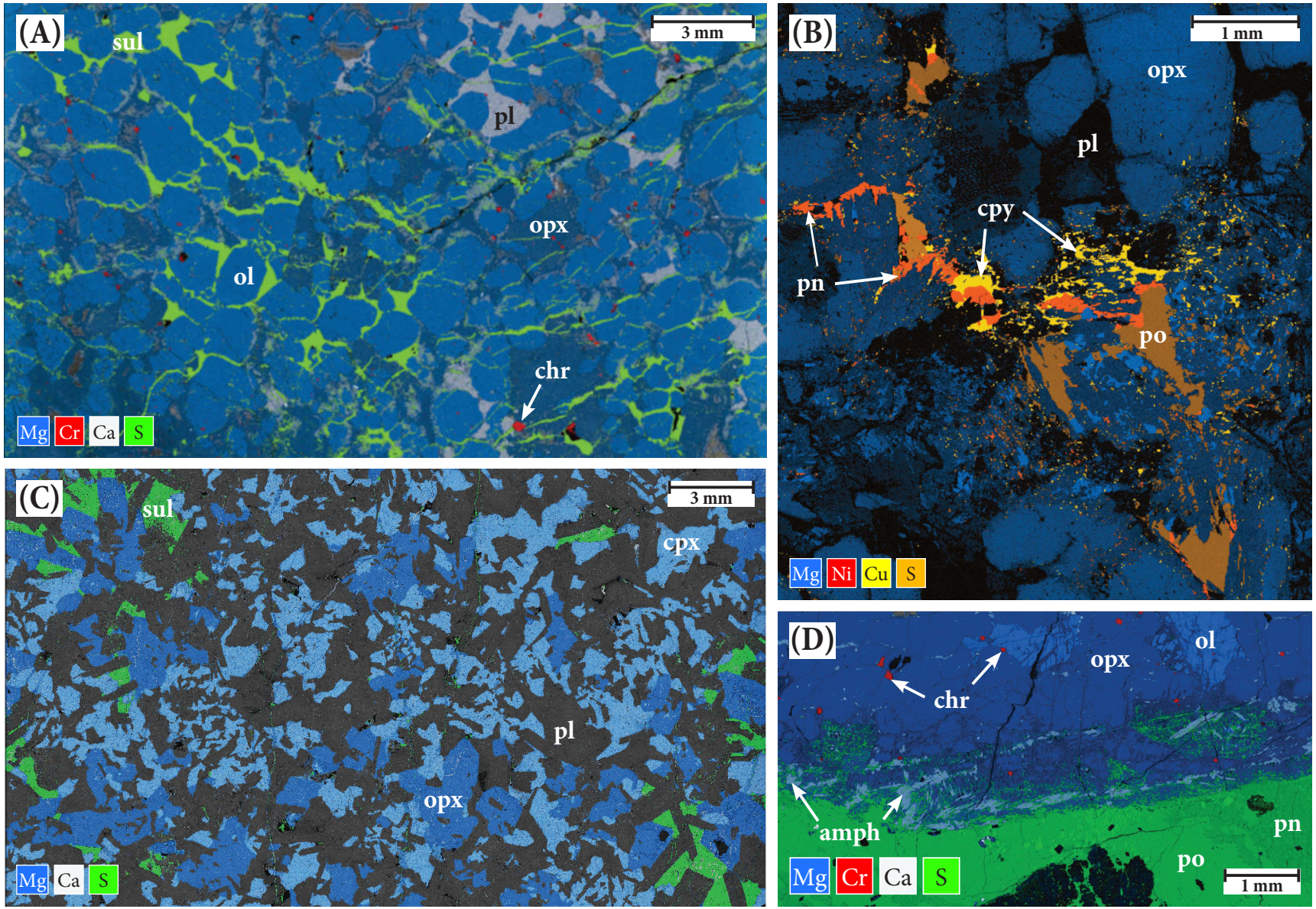
(A)
sul
3 mm
pl
opx
ol
chr
Mg
Cr
Ca
S
(B)
1 mm
opx
pl
cpy
pn
po
Mg
Ni
Cu
S
(C)
sul
3 mm
cpx
pl
opx
Mg
Ca
S
(D)
ol
opx
chr
amph
pn
po
Mg
Cr
Ca
S
1 mm

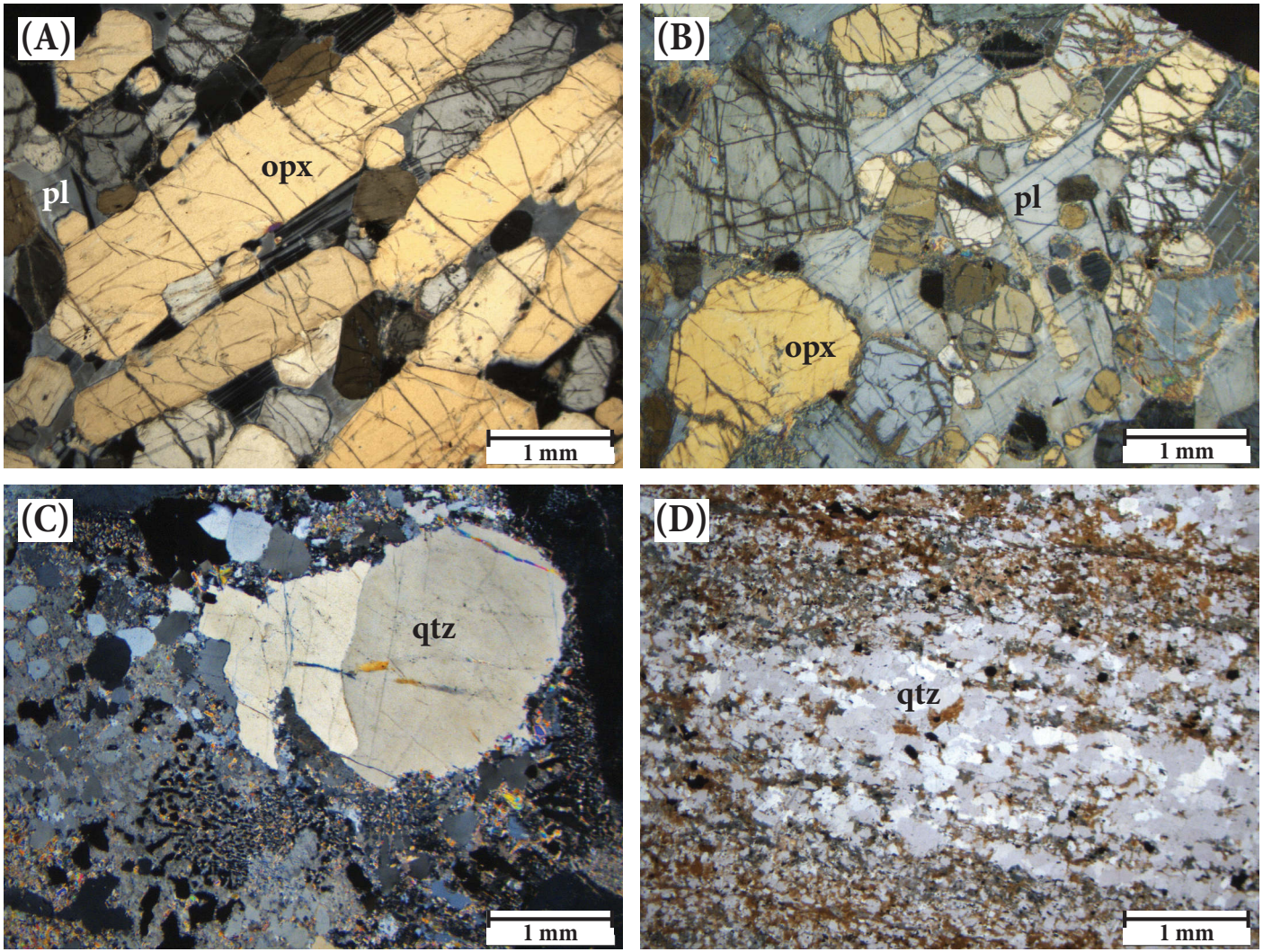
(A)
opx
pl
1 mm
(B)
pl
opx
1 mm
(C)
qtz
1 mm
(D)
qtz
1 mm

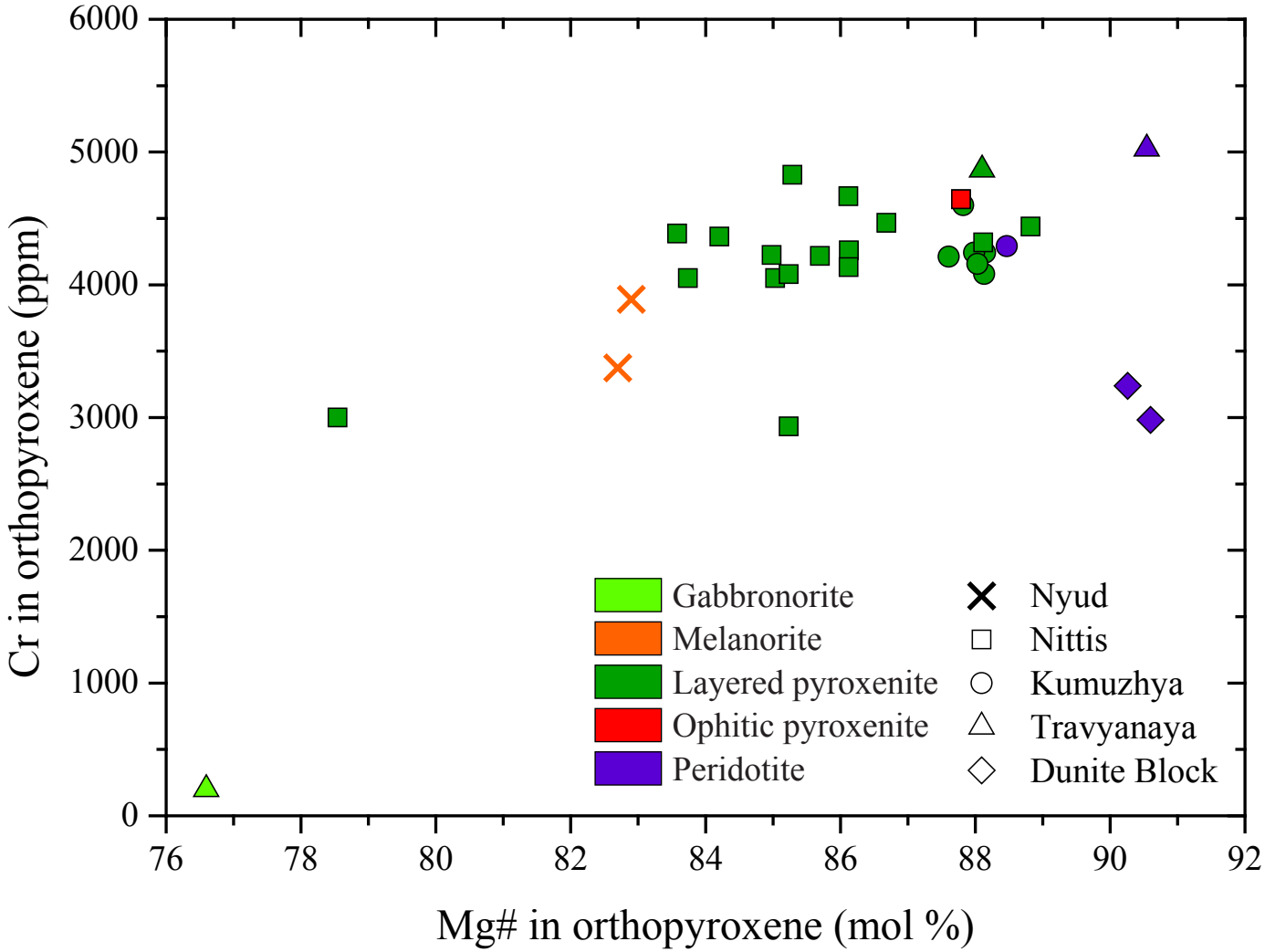
6000
5000
4000
3000
2000
1000
0
Cr in orthopyroxene (ppm)
76
78
80
82
84
86
88
90
92
Mg# in orthopyroxene (mol %)
Gabbronorite
Melanorite
Layered pyroxenite
Ophitic pyroxenite
Peridotite
Nyud
Nittis
Kumuzhya
Travyanaya
Dunite Block

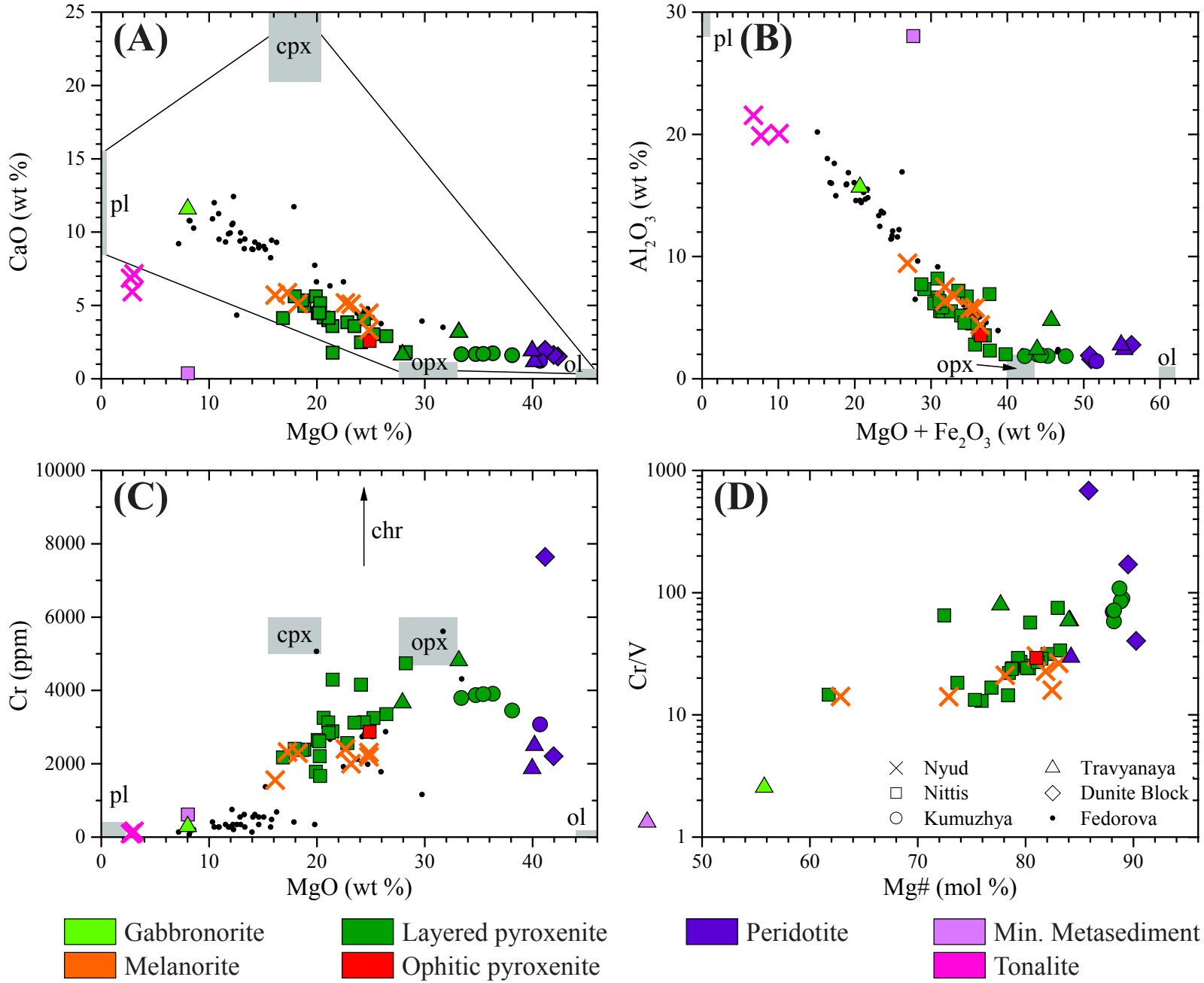
(A)
cpx
pl
opx
ol
CaO (wt %)
MgO (wt %)
(B)
pl
opx
ol
Al2O3 (wt %)
MgO + Fe2O3 (wt %)
(C)
chr
cpx
opx
pl
ol
Cr (ppm)
MgO (wt %)
(D)
Cr/V
Mg# (mol %)
Nyud
Nittis
Kumuzhya
Travyanaya
Dunite Block
Fedorova
Gabbronorite
Melanorite
Layered pyroxenite
Ophitic pyroxenite
Peridotite
Min. Metasediment
Tonalite

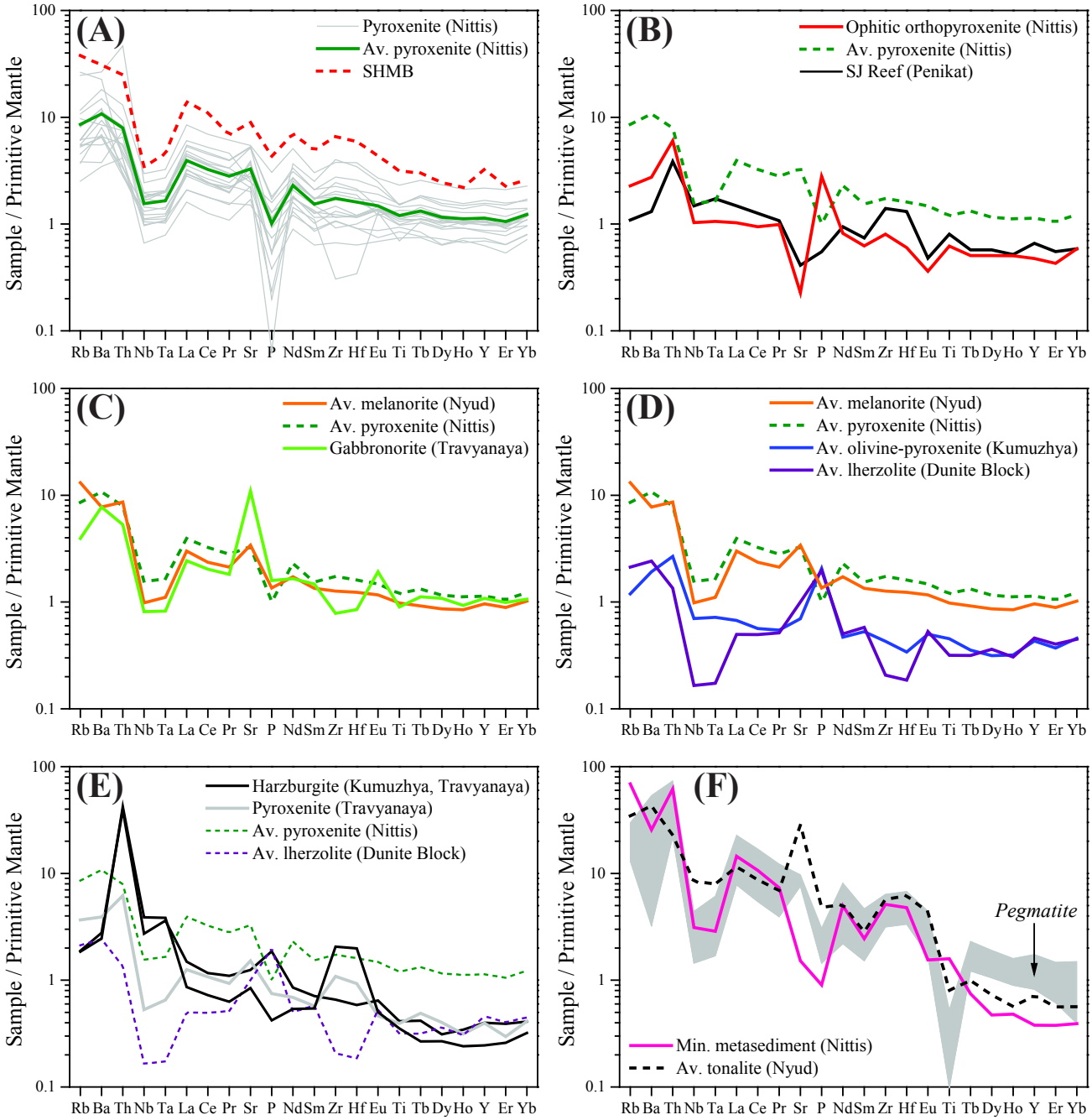
(A)
Pyroxenite (Nittis)
Av. pyroxenite (Nittis)
SHMB
(B)
Ophitic orthopyroxenite (Nittis)
Av. pyroxenite (Nittis)
SJ Reef (Penikat)
(C)
Av. melanorite (Nyud)
Av. pyroxenite (Nittis)
Gabbronorite (Travyanaya)
(D)
Av. melanorite (Nyud)
Av. pyroxenite (Nittis)
Av. olivine-pyroxenite (Kumuzhya)
Av. lherzolite (Dunite Block)
(E)
Harzburgite (Kumuzhya, Travyanaya)
Pyroxenite (Travyanaya)
Av. pyroxenite (Nittis)
Av. lherzolite (Dunite Block)
(F)
Pegmatite
Min. metasediment (Nittis)
Av. tonalite (Nyud)
Sample / Primitive Mantle
100
10
1
0.1
Rb Ba Th Nb Ta La Ce Pr Sr P Nd Sm Zr Hf Eu Ti Tb Dy Ho Y Er Yb

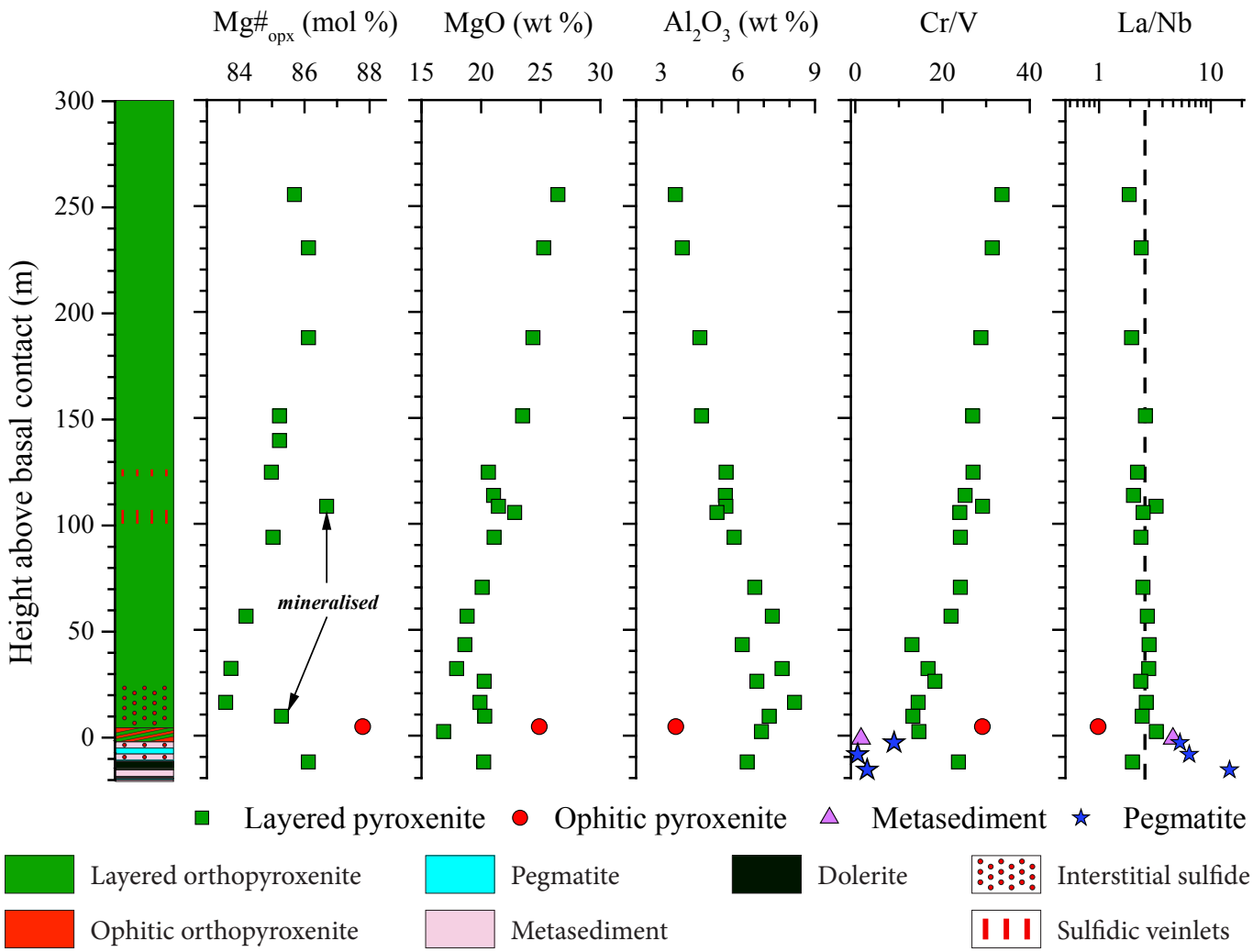
Mg#opx (mol %)
MgO (wt %)
Al2O3 (wt %)
Cr/V
La/Nb
84
86
88
15
20
25
30
3
6
9
0
20
40
1
10
300
250
200
150
100
50
0
Height above basal contact (m)
mineralised
Layered pyroxenite
Ophitic pyroxenite
Metasediment
Pegmatite
Layered orthopyroxenite
Ophitic orthopyroxenite
Pegmatite
Metasediment
Dolerite
Interstitial sulfide
Sulfidic veinlets

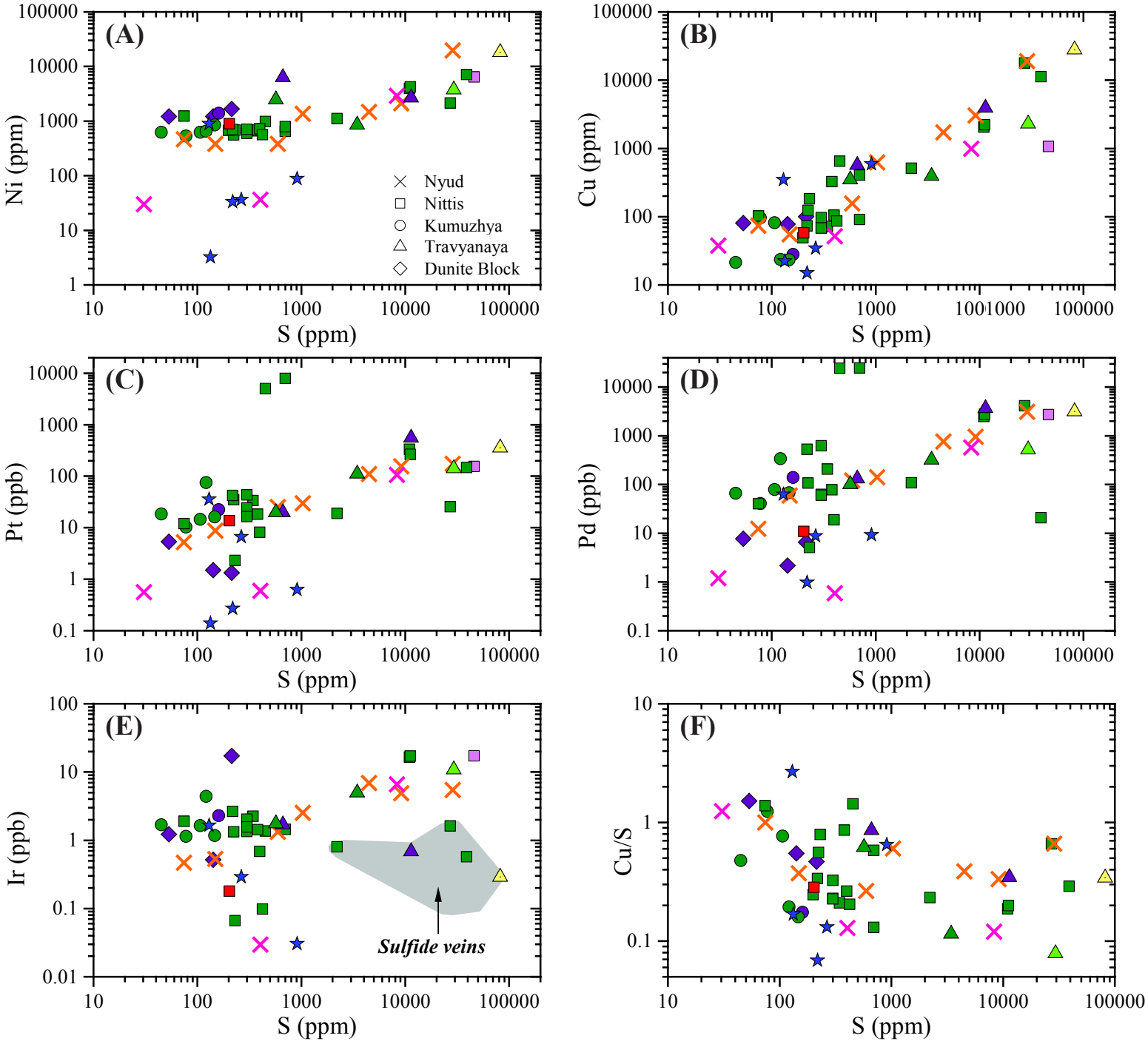
(A)
Ni (ppm)
S (ppm)
Nyud
Nittis
Kumuzhya
Travyanaya
Dunite Block
(B)
Cu (ppm)
S (ppm)
(C)
Pt (ppb)
S (ppm)
(D)
Pd (ppb)
S (ppm)
(E)
Ir (ppb)
Sulfide veins
S (ppm)
(F)
Cu/S
S (ppm)
Gabbronorite
Melanorite
Layered pyroxenite
Ophitic pyroxenite
Peridotite
Massive sulfide
Tonalite
Min. Metasediment
Pegmatite

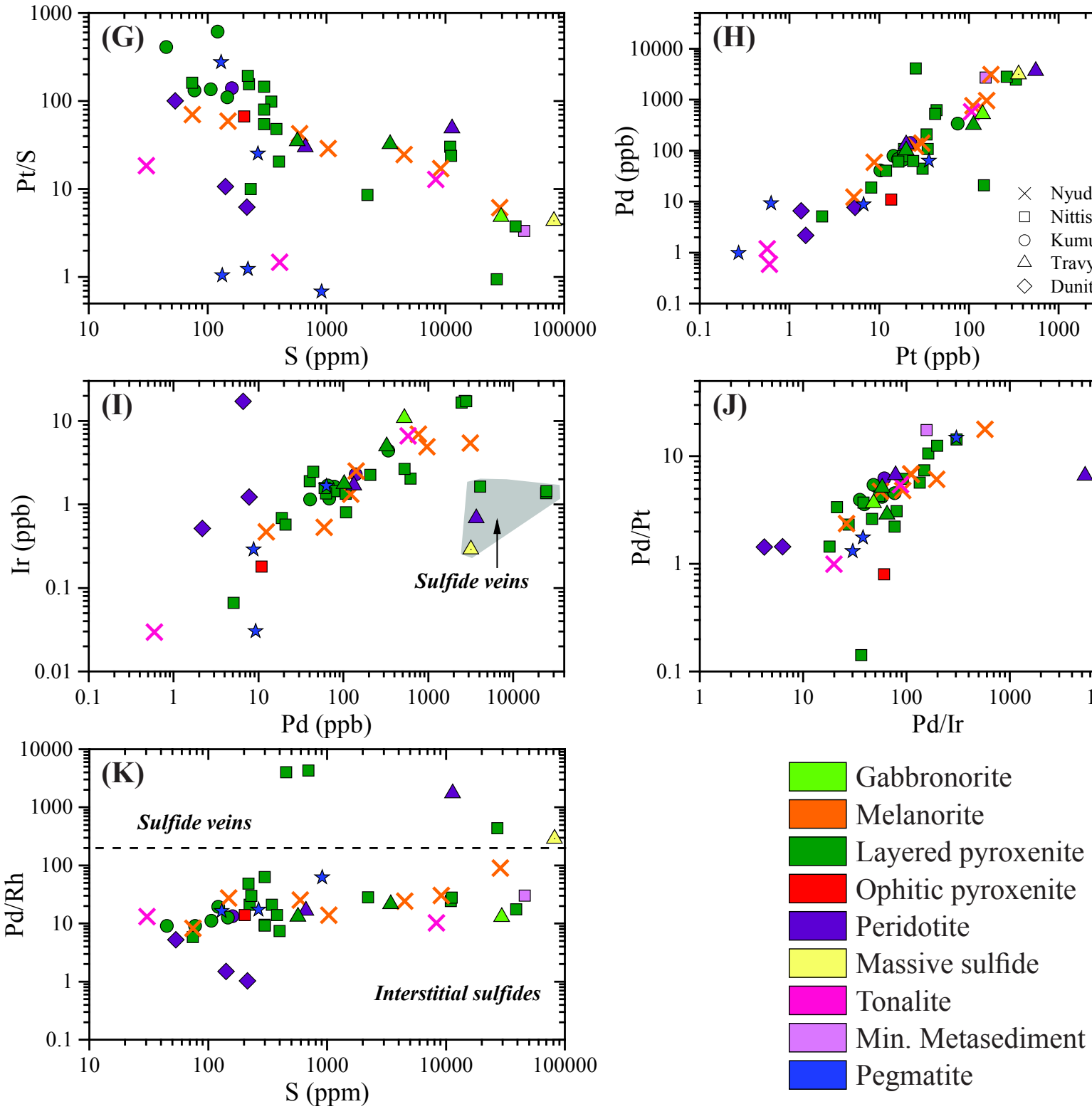
(G)
Pt/S
S (ppm)
(H)
Pd (ppb)
Pt (ppb)
Nyud
Nittis
Kumuzhya
Travyanaya
Dunite Block
(I)
Ir (ppb)
Pd (ppb)
Sulfide veins
(J)
Pd/Pt
Pd/Ir
(K)
Pd/Rh
S (ppm)
Sulfide veins
Interstitial sulfides
Gabbronorite
Melanorite
Layered pyroxenite
Ophitic pyroxenite
Peridotite
Massive sulfide
Tonalite
Min. Metasediment
Pegmatite

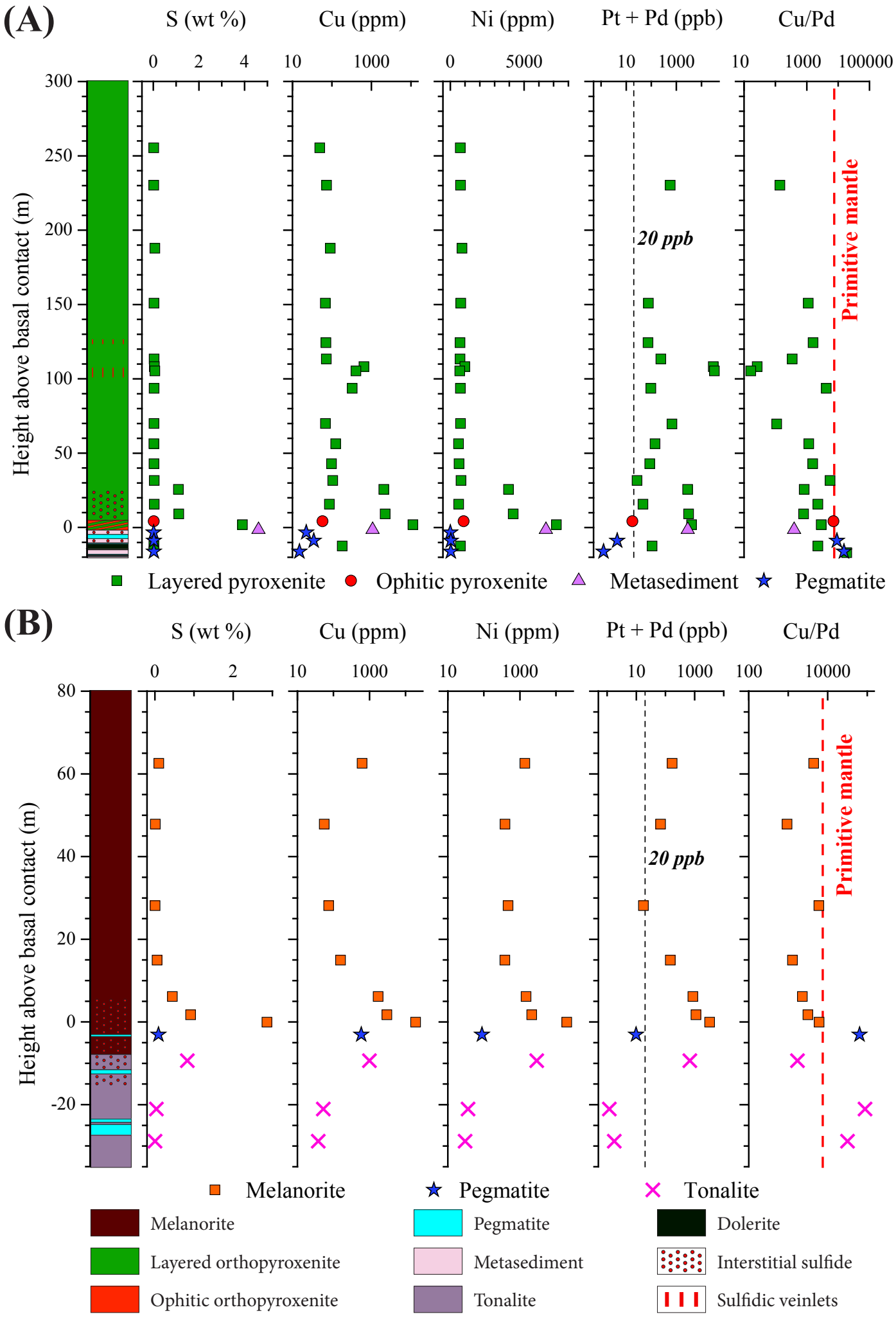
(A)
S (wt %)
Cu (ppm)
Ni (ppm)
Pt + Pd (ppb)
Cu/Pd
0
2
4
10
1000
0
5000
10
1000
10
1000
100000
300
250
200
150
100
50
0
Height above basal contact (m)
20 ppb
Primitive mantle
Layered pyroxenite
Ophitic pyroxenite
Metasediment
Pegmatite
(B)
S (wt %)
Cu (ppm)
Ni (ppm)
Pt + Pd (ppb)
Cu/Pd
0
2
10
1000
10
1000
10
1000
100
10000
80
60
40
20
0
-20
Height above basal contact (m)
20 ppb
Primitive mantle
Melanorite
Pegmatite
Tonalite
Melanorite
Layered orthopyroxenite
Ophitic orthopyroxenite
Pegmatite
Metasediment
Tonalite
Dolerite
Interstitial sulfide
Sulfidic veinlets

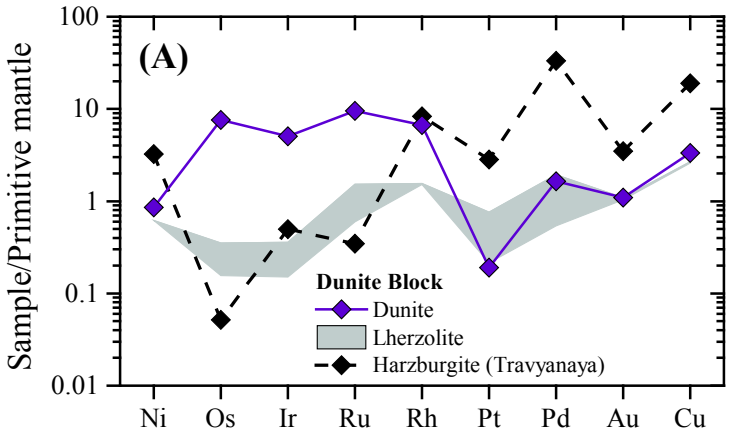
(A)
Sample/Primitive mantle
100
10
1
0.1
0.01
Ni Os Ir Ru Rh Pt Pd Au Cu
Dunite Block
Dunite
Lherzolite
Harzburgite (Travyanaya)

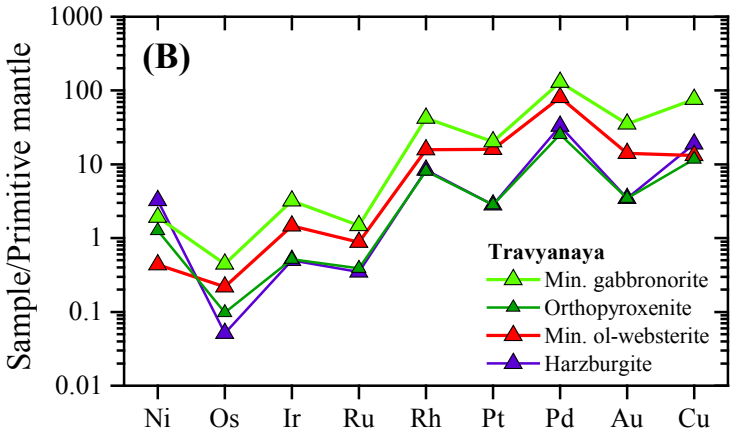
(B)
Sample/Primitive mantle
1000
100
10
1
0.1
0.01
Ni Os Ir Ru Rh Pt Pd Au Cu
Travyanaya
Min. gabbronorite
Orthopyroxenite
Min. ol-websterite
Harzburgite

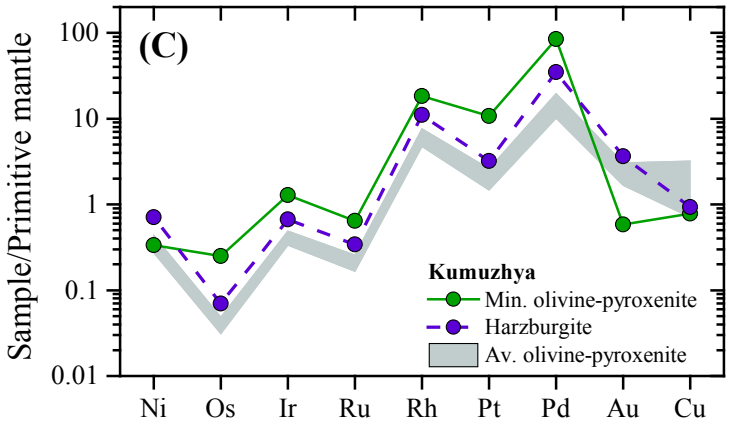
(C)
Sample/Primitive mantle
100
10
1
0.1
0.01
Ni Os Ir Ru Rh Pt Pd Au Cu
Kumuzhya
Min. olivine-pyroxenite
Harzburgite
Av. olivine-pyroxenite

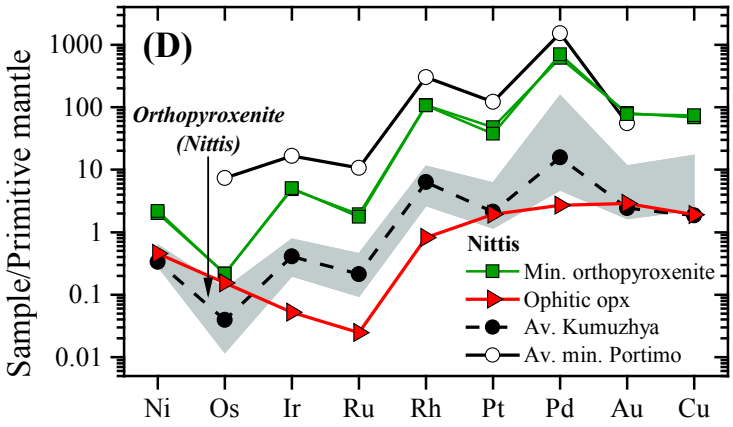
(D)
Sample/Primitive mantle
1000
100
10
1
0.1
0.01
Ni Os Ir Ru Rh Pt Pd Au Cu
Orthopyroxenite
(Nittis)
Nittis
Min. orthopyroxenite
Ophitic opx
Av. Kumuzhya
Av. min. Portimo

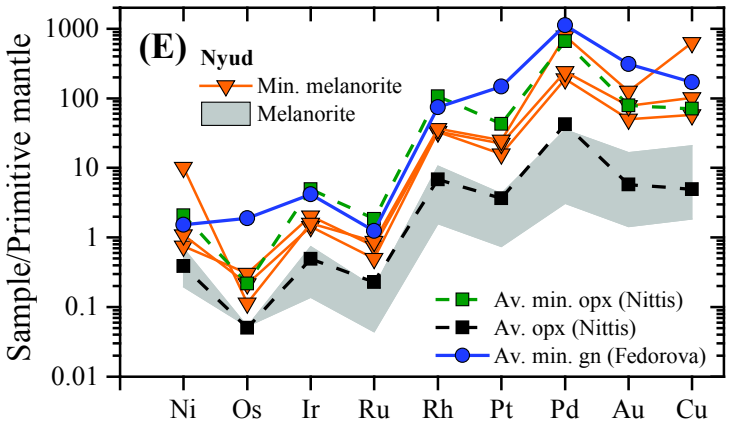
(E)
Sample/Primitive mantle
1000
100
10
1
0.1
0.01
Ni Os Ir Ru Rh Pt Pd Au Cu
Nyud
Min. melanorite
Melanorite
Av. min. opx (Nittis)
Av. opx (Nittis)
Av. min. gn (Fedorova)

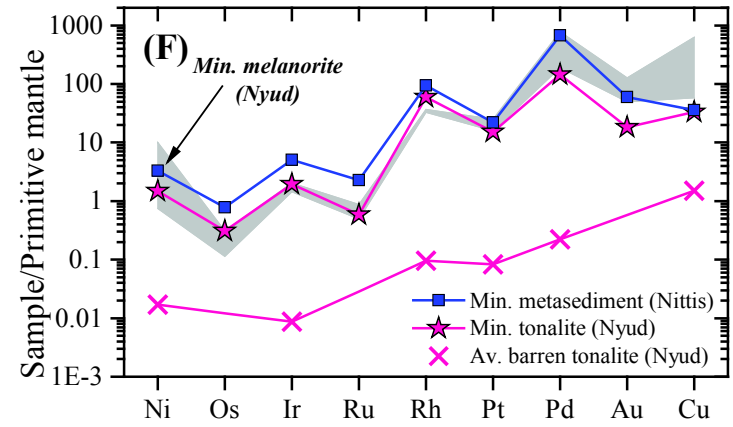
(F)
Sample/Primitive mantle
1000
100
10
1
0.1
0.01
1E-3
Ni Os Ir Ru Rh Pt Pd Au Cu
Min. melanorite
(Nyud)
Min. metasediment (Nittis)
Min. tonalite (Nyud)
Av. barren tonalite (Nyud)

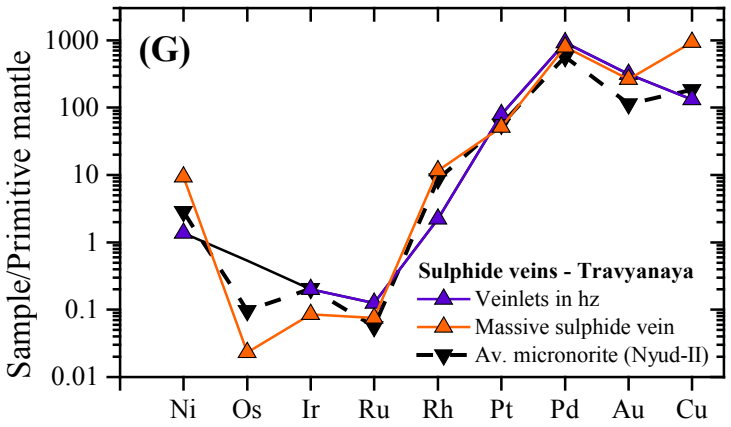
(G)
Sample/Primitive mantle
1000
100
10
1
0.1
0.01
Ni Os Ir Ru Rh Pt Pd Au Cu
Sulphide veins - Travyanaya
Veinlets in hz
Massive sulphide vein
Av. micronorite (Nyud-II)

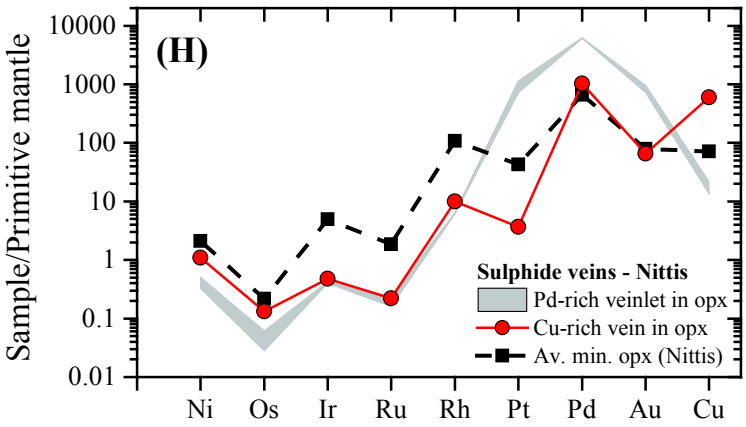
(H)
Sample/Primitive mantle
10000
1000
100
10
1
0.1
0.01
Ni Os Ir Ru Rh Pt Pd Au Cu
Sulphide veins - Nittis
Pd-rich veinlet in opx
Cu-rich vein in opx
Av. min. opx (Nittis)

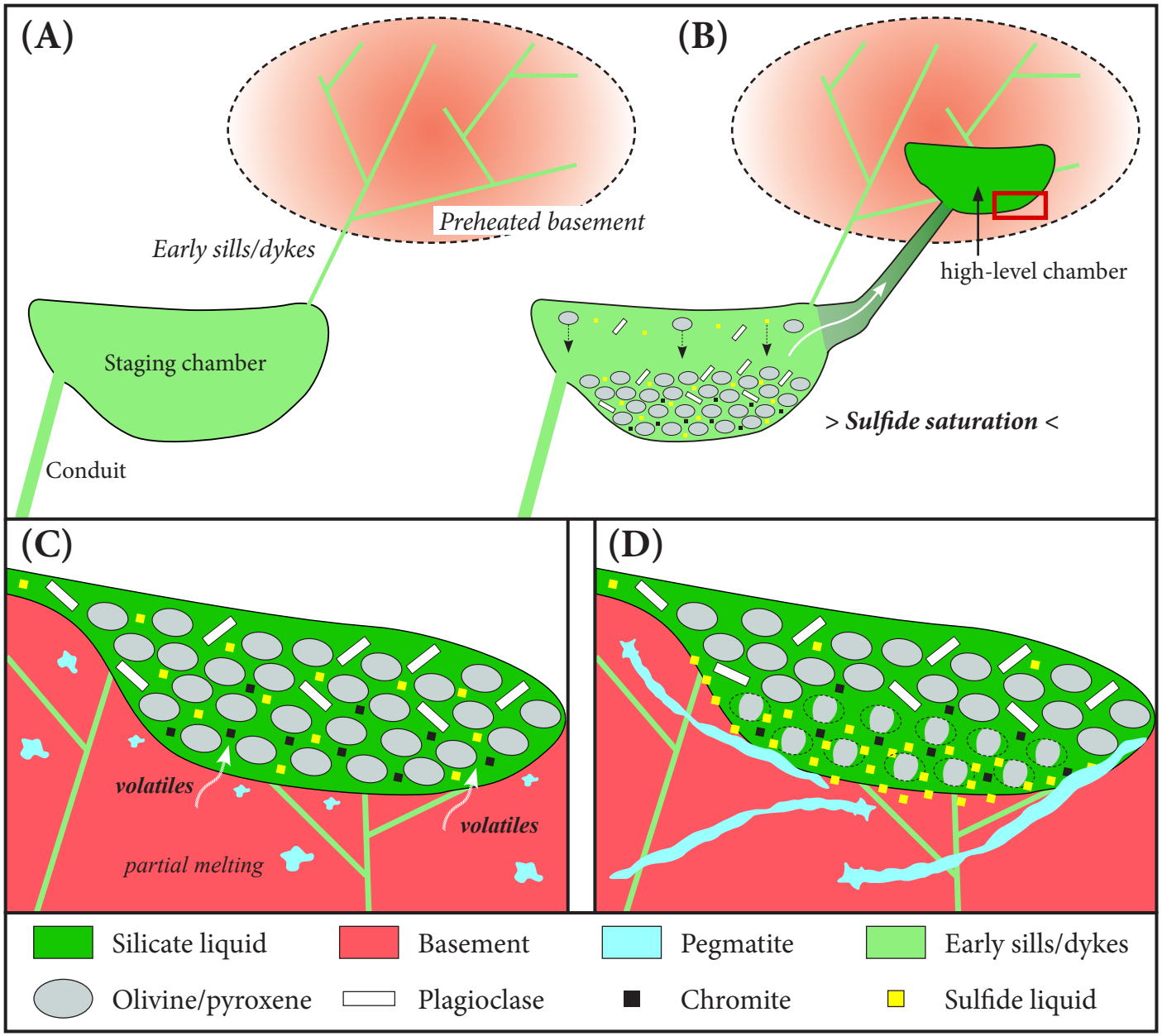
(A)
(B)
Preheated basement
Early sills/dykes
Staging chamber
Conduit
high-level chamber
> Sulfide saturation <
(C)
(D)
volatiles
volatiles
partial melting
Silicate liquid
Basement
Pegmatite
Early sills/dykes
Olivine/pyroxene
Plagioclase
Chromite
Sulfide liquid

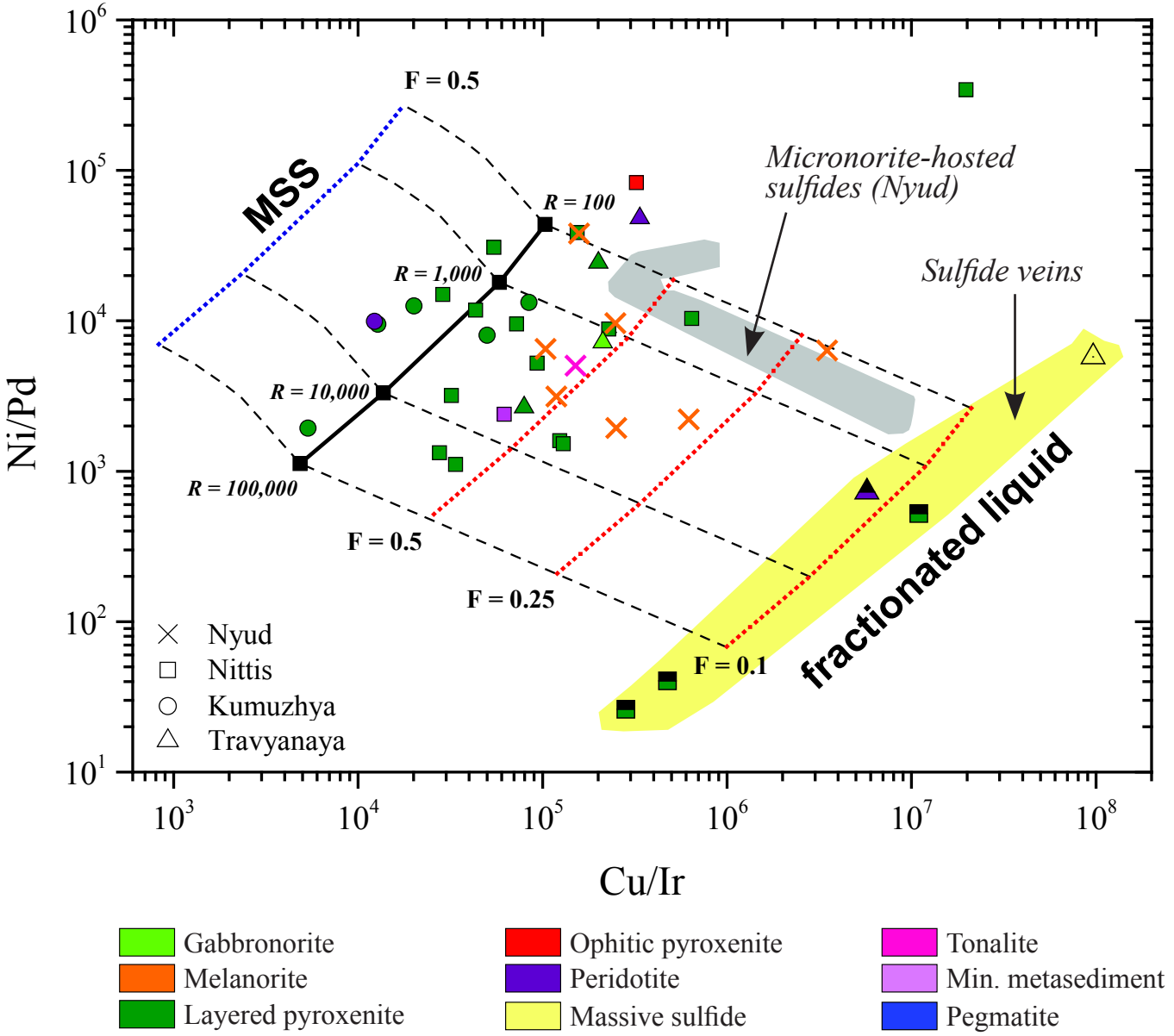
Ni/Pd
Cu/Ir
MSS
F = 0.5
R = 100
R = 1,000
R = 10,000
R = 100,000
F = 0.5
F = 0.25
F = 0.1
Micronorite-hosted sulfides (Nyud)
Sulfide veins
fractionated liquid
Nyud
Nittis
Kumuzhya
Travyanaya
Gabbronorite
Melanorite
Layered pyroxenite
Ophitic pyroxenite
Peridotite
Massive sulfide
Tonalite
Min. metasediment
Pegmatite

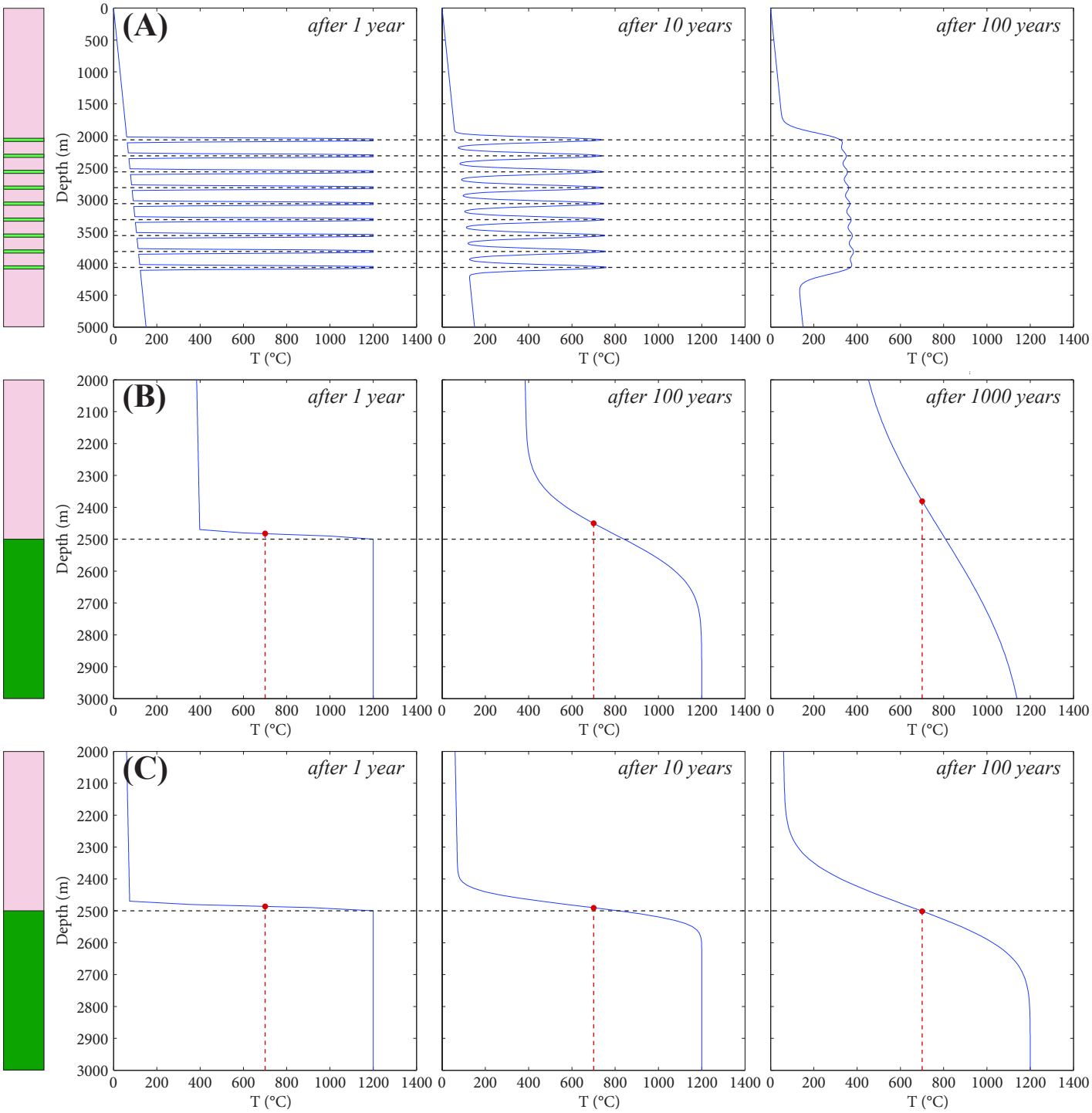
(A)
after 1 year
after 10 years
after 100 years
Depth (m)
T (°C)
(B)
after 1 year
after 100 years
after 1000 years
Depth (m)
T (°C)
(C)
after 1 year
after 10 years
after 100 years
Depth (m)
T (°C)

Table 1 Comparison of results obtained at LabMaTer and the accepted values for international standards

	KPT				LK-NIP			WMS-1a						Blank	
	LabMaTer (n = 8)		LabMaTer		LabMaTer (n = 7)		Geolabs	LabMaTer (n = 2)		LabMaTer		CANMET		LabMaTer (n = 36)	
	This run	1 sigma	working value[a]	1 sigma	This run	1 sigma	Certificate	This run	1 sigma	working value[a]	1 sigma	Certificate	1 sigma	This run	1 sigma
Os (ppb)	2.08	0.43	2.80	0.19	0.01	0.02	n.v.	120.00	1.94	135.40	4.60	150.00	n.v.	0.18	0.06
Ir	5.98	0.91	6.62	0.74	0.17	0.01	0.19	337.01	3.08	338.50	4.50	322.00	10.00	0.01	0.01
Ru	15.93	0.59	16.85	0.93	0.45	0.04	0.44	143.98	2.35	147.10	1.30	145.00	7.00	0.03	0.01
Rh	14.09	1.51	15.35	1.24	0.85	0.06	0.90	254.30	3.51	254.60	2.90	222.00	15.00	0.02	0.01
Pt	103.91	28.68	97.40	20.99	12.79	0.76	13.43	1962.89	35.18	2032.00	45.40	1910.00	70.00	0.12	0.06
Pd	121.51	18.95	123.40	18.60	16.18	1.44	17.96	1572.23	24.49	1534.30	36.12	1450.00	50.00	0.51	0.19
Au	40.71	8.49	37.33	11.55	4.26	1.05	4.63	220.65	1.92	311.60	30.80	300.00	43.00	1.23	0.16

KPT = Quartz diorite (in-house LabMaTer)

LK-NIP = Nipigon Diabase (Geolabs)

WMS-1a = Wellgreen massive sulfide (CANMET)

[a] = Savard et al. (2010)

n.v. = no value

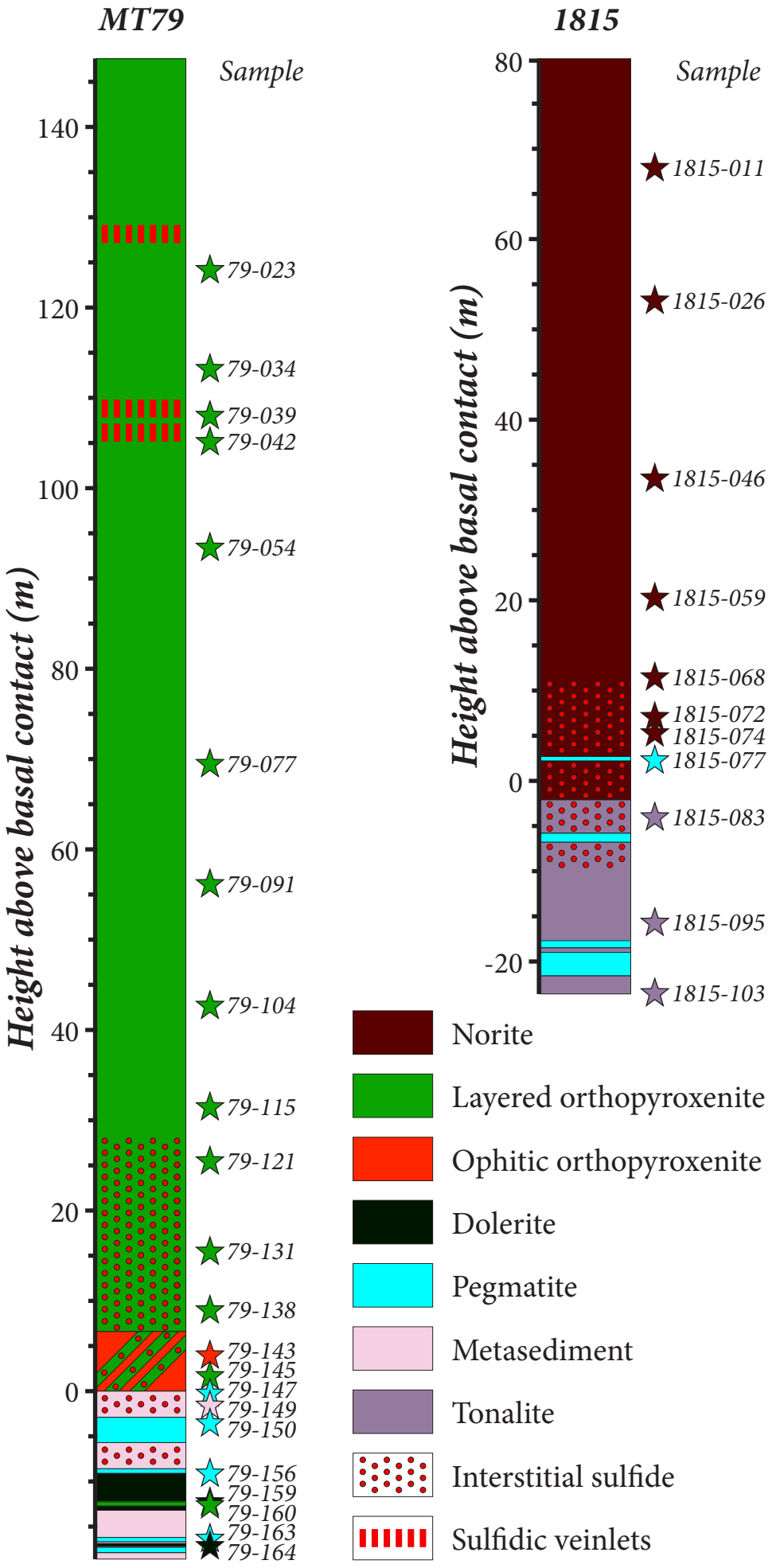
MT79
Sample
Height above basal contact (m)
140
120
100
80
60
40
20
0
79-023
79-034
79-039
79-042
79-054
79-077
79-091
79-104
79-115
79-121
79-131
79-138
79-143
79-145
79-147
79-149
79-150
79-156
79-159
79-160
79-163
79-164
1815
Sample
Height above basal contact (m)
80
60
40
20
0
-20
1815-011
1815-026
1815-046
1815-059
1815-068
1815-072
1815-074
1815-077
1815-083
1815-095
1815-103
Norite
Layered orthopyroxenite
Ophitic orthopyroxenite
Dolerite
Pegmatite
Metasediment
Tonalite
Interstitial sulfide
Sulfidic veinlets

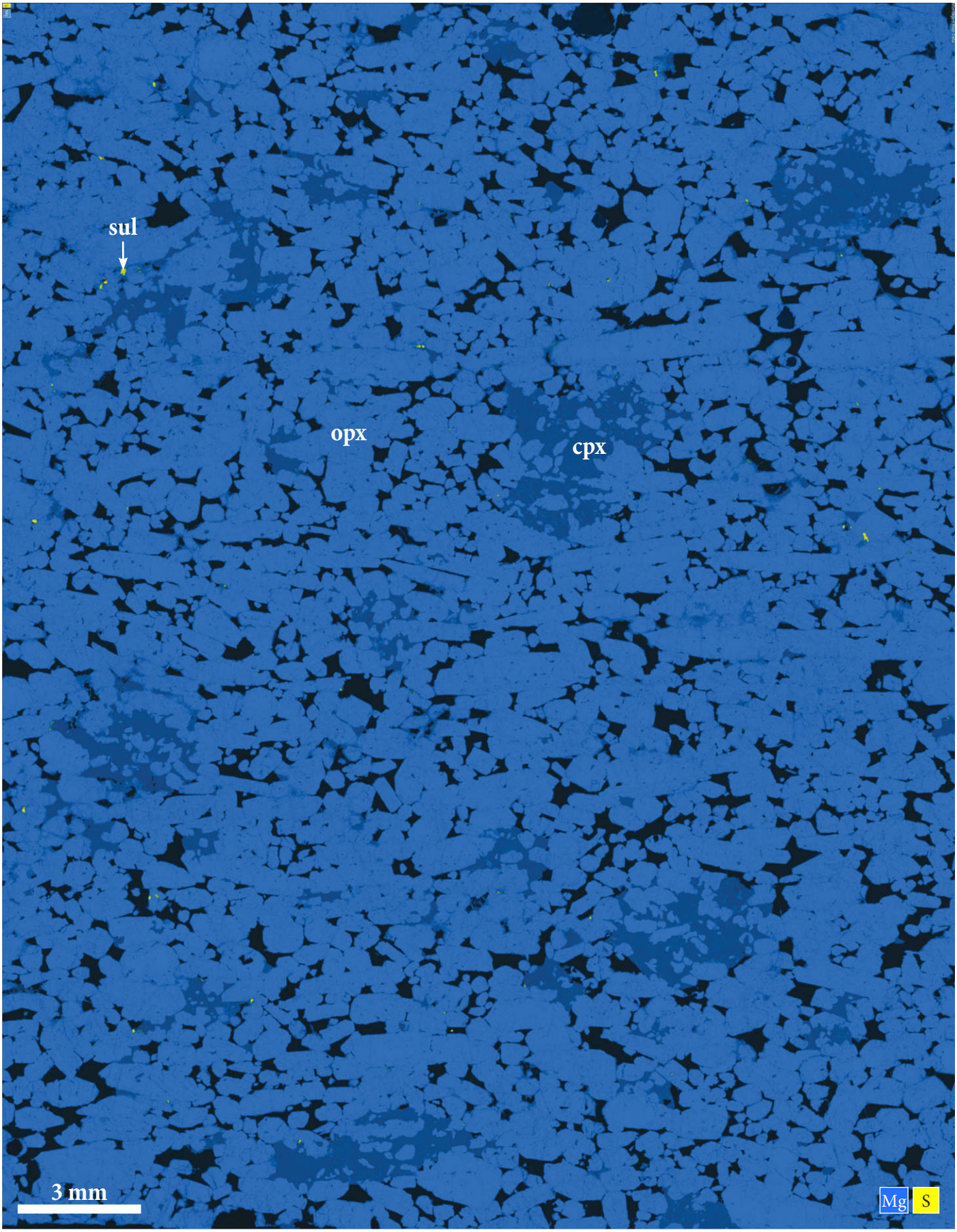
sul
opx
cpx
3 mm
Mg
S

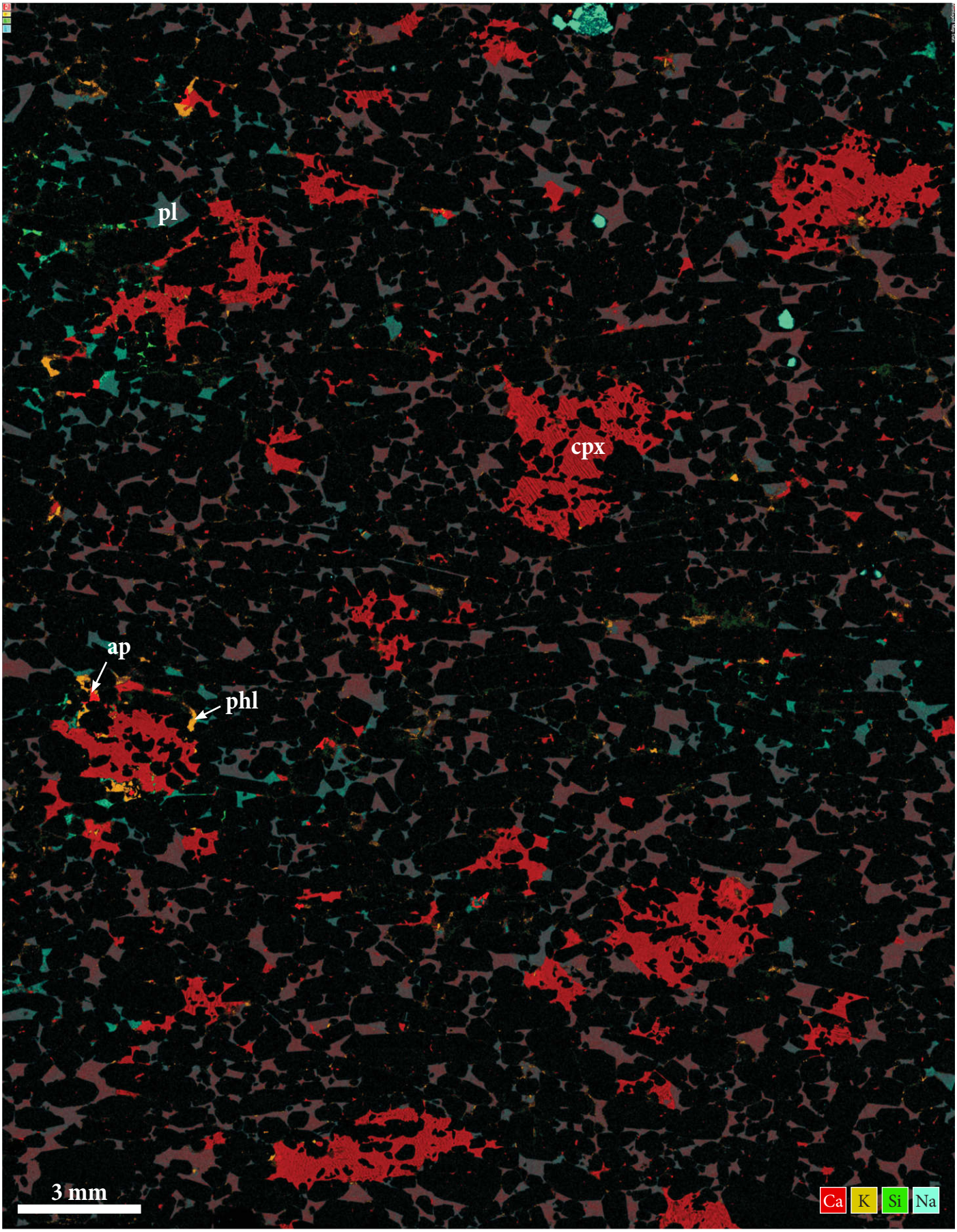
pl
cpx
ap
phl
3 mm
Ca
K
Si
Na